AALBORG UNIVERSITY

Assessment of Smooth Muscle Cell Differentiation and Cell-laden Biomaterials Properties for Urethral Reconstruction

Master's Thesis

in

Medicine with Industrial Specialization
Department of Health Science and Technology

Author: Pitsa Aikaterini-Chara
Supervisor: Cristian Pablo Pennisi
Project Period: 1st September 2018- 30th May 2019

30/05/2019

Preface

The IEEE method was used for citation within the present thesis. Figures without references are made by the author of this thesis.

The author would like to thank the research supervisor Cristian Pablo Pennisi for his constructive guidance and support during this project. His interest, patience and welcoming nature throughout this work were precious. The author would also like to express appreciation to technicians Lisa Engen and Ole Jensen for being supportive and always willing to assist.

Table of Contents

Abstract

Urethral stricture disease is a common condition, resulting from urethral injuries, which affects primarily the male population. To date, the treatment options for long (>2cm) urethral strictures in men are insufficient. Urethral tissue engineering has emerged as a potential approach to treat long urethral strictures in which the treatments approaches have the lowest success rate. In principle, tissue engineering aims to develop biological substitutes which can recapitulate the unique features and functions of tissues and organs based on the right combination of biomaterials and cell sources. However, the fabrication of a fully functional biological construct in the field of urethral reconstruction remains a challenge. The aim of this project is to assess the smooth muscle cells (SMCs) as a potential cell source for urethral reconstruction based on their differentiation capacity and compare the ability of two different SMCs-laden biomaterials; CELLINK and Lifeink® 200 to be extruded into three-dimensional (3D) constructs mimicking the biological properties of an urethral environment. For the induction of differentiation in SMCs, a differentiation medium based on heparin was composed. The differentiation of SMCs was evaluated at transcriptional level by real time reverse transcription polymerase chain reaction (RT-qPCR) and at translational level by immunofluorescence staining. Moreover, a carbachol contraction assay was performed. For the fabrication of the 3D constructs, the 3D bioprinting technology was utilized. The effect of the biomaterials on the SMCs behavior was investigated by Live/Dead staining, Alamar blue assay, elastin staining and RT-qPCR. In this study, the results obtained from the RT-qPCR, immunofluorescence staining and carbachol contraction did not indicate differentiation of SMCs. Therefore, future studies should focus on other mediators of SMC differentiation such as different soluble factors. In addition, between CELLINK and Lifeink® 200, the second found to be more suitable for the biofabrication of bioprinted cell-laden constructs indicating a potential biomaterial candidate for the urethral reconstruction.

Abbreviations

TE	Tissue Engineering
3D	Three-dimensional
ECM	Extracellular matrix
GAGs	Glycosaminoglycans
SMCs	Smooth muscle cells
TGF-β1	Transforming growth factor β1
Ca^{2+}	Calcium ions
SR	Sarcoplasmic Reticulum
CaM	Calmodulin
MLCK	Myosin light chain kinase
α-SMA	α-smooth muscle actin
MHC	Myosin heavy chain
MLC	Myosin light chain
CaD	Caldesmon
h-Cad	Heavy isoform of caldesmon
l-Cad	Light isoform of caldesmon
GelMA	Gelatin methacryloyl
PCL	Poly (ε-caprolactone)
PLCL	Poly(lactide-co-caprolactone)
HUSMCs	Human urothelial smooth muscle cells
FBS	Fetal Bovine Serum
EGF	Epidermal growth factor
FGF-b	Fibroblast growth factor-basic
GM	Growth medium
2D	Two-dimensional
DM	Differentiation medium
RT-qPCR	Real time reverse transcription polymerase chain reaction
cDNA	Complementary DNA
PBS	Phosphate buffered saline
PPIA	Peptidylprolyl Isomerase A
YWHAZ	Tyrosine 3-Monooxygenase/Tryptophan 5-Monooxygenase Activation Protein Zeta
AB	Alamar blue
PFA	Paraformaldehyde
SD	Standard deviation
RFU	Relative fluorescence units

1. Introduction

Urethral stricture is a common condition resulting from urethral injuries and it is characterized by a narrowing of the urethral lumen due to the presence of scar tissue. Urethral stricture affects primarily the male population and its estimated prevalence among men is 0.6% [1]. The etiology of this condition varies across patients as the stricture can occur after an infection or inflammatory disease, during a diagnostic or therapeutic procedure, but it has also been associated with idiopathic and traumatic causes. Most men experiencing a stricture will typically present with voiding and storage dysfunction but over time, they may be at risk of serious complications such as urinary tract infections which can lead to prostatitis or kidney damage. Undeniably, all these conditions can impose a significant burden not only on their health but also on their quality of life [2]. Currently, several treatments are available for the management of urethral strictures. However, as the success rate remains low, a novel and effective treatment of urethral strictures needs to be explored. The field of tissue engineering (TE) and the advent of new technologies such as the three-dimensional (3D) bioprinting technology seems to hold great promise [3].

1.1 Anatomy and histology of the male urethra

The lower urinary tract consists of the urinary bladder, the urethra and the urinary sphincters. Its main function includes the storage and expulsion of urine produced by the kidneys. In both males and females, the expulsion of urine from the body is mediated by the urethra, a distensible tubular structure. Furthermore, urethra serves as an outlet for the seminal fluids in men [4].
The male urethra is between 13 and 20cm long and it can be divided into the posterior and anterior urethra [5], [6]. The posterior urethra is subdivided into the prostatic and membranous urethra, whereas the anterior comprises the bulbar and the penile parts. The prostatic urethra has a length of 3-4 cm, is connected to the bladder neck and courses through the prostate. Immediately upon emerging from the prostate, the urethra is referred as the membranous urethra which is the shortest segment of the urethra and the least dilatable. The bulbar part of urethra is located right after the urogenital diaphragm and it extends through the pelvic floor where it is continuous with the penile urethra. The penile segment is the last and the longest portion of the urethra, as it is approximately 15 cm in length, and extends along the shaft of the penis [6], [7]. Together, the bulbar and the penile urethra comprise the spongy urethra which is surrounded by the corpus spongiosum (Figure 1) [5], [6].

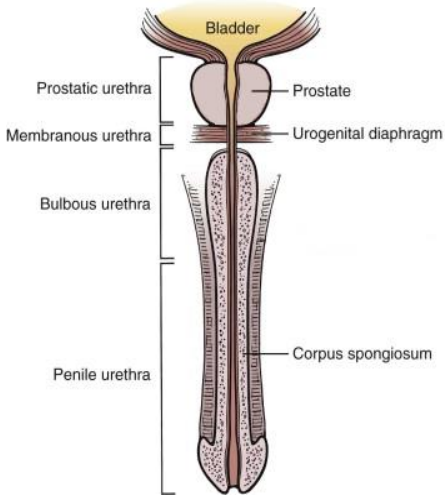

Figure 1: Anatomy of the male urethra. Modified from [8]

The urethral tube is a multi-layered tissue consisting of three layers: the urethral epithelium which lines the lumen of urethra and it is surrounded by a collagenous connective tissue, the lamina propria and the smooth muscle layer. The epithelial lining of the male urethra varies along the different segments of urethra. More specifically, the prostatic urethra is lined with the transitional epithelium called urothelium whereas the membranous and the spongy parts of urethra are lined with pseudostratified columnar epithelium [9]. All the layers of urethra are covered by an extracellular matrix (ECM), a structural scaffold made up of proteins such as collagen I and III, elastin, proteoglycans and glycosaminoglycans (GAGs) [10].

1.1.1 Urethral smooth muscle layer

The smooth muscle tissue in urethra comprises two distinct smooth muscle layers: an inner layer of longitudinally arranged smooth muscle cells (SMCs) and outside this, a circular smooth muscle layer. During micturition, the longitudinal layer contracts and the urethra shortens whereas during the filling phase, the contraction of the circular smooth muscle layer contribute to an effective constriction of the urethra. The mechanical activity of the smooth muscle layer in urethra is controlled by the sympathetic and parasympathetic systems [11]. Furthermore, the ECM overlaying the smooth muscle layer contributes to the mechanical deformations of the urethra. Collagen provides structure and tensile strength to the urethra while elastin is important for the urethral compliance due to its high degree of extensibility [10].

1.1.2 SMC characteristics

SMCs present a phenotypic diversity as they can switch from a synthetic to a contractile phenotype, and vice versa. In primary cultures, SMCs can switch from a synthetic to a differentiated contractile phenotype, a shift which is described as maturation. This phenotypic change is mediated by the expression of specific SMCs marker genes and it is characterized by differences in morphology and the proliferative properties of SMCs. Contractile SMCs appear as elongated, spindle-shaped cells whereas synthetic SMCs exhibit a rhomboid morphology. Furthermore, synthetic SMCs demonstrate a high proliferative, migratory and ECM synthesis rate while in contrast contractile SMCs present a low capacity of proliferation, migration and secretion of ECM [12], [13]. In this phenotypic plasticity, signaling molecules such as the transforming growth factor beta 1 (TGF-β1) or heparin play a pivotal role. For instance, in vascular SMCs, TGF-

β1 induces phenotypical changes to SMCs towards a contractile phenotype as it regulates transcriptionally the expression of several SMC genes [13].
In SMCs, the contractile activity is initiated by a calcium influx and it is regulated primarily by the contractile proteins, actin and myosin. Once calcium has entered the cell, it triggers the release of calcium ions (Ca^{2+}) from the sarcoplasmic reticulum (SR). As a result, the intracellular concentration of Ca^{2+} is increased. The intracellular Ca^{2+} then bind to a protein called calmodulin (CaM), which in turn activates the enzyme myosin light chain kinase (MLCK) instigating the phosphorylation of the myosin regulatory light chain. The phosphorylation of the myosin regulatory light chain leads to the activation of the myosin ATPase which allows the cross-bridge formation between actin and myosin. Hence, the cross-bridge cycling occurs, and the smooth muscle contraction is generated (Figure 2) [14], [15].

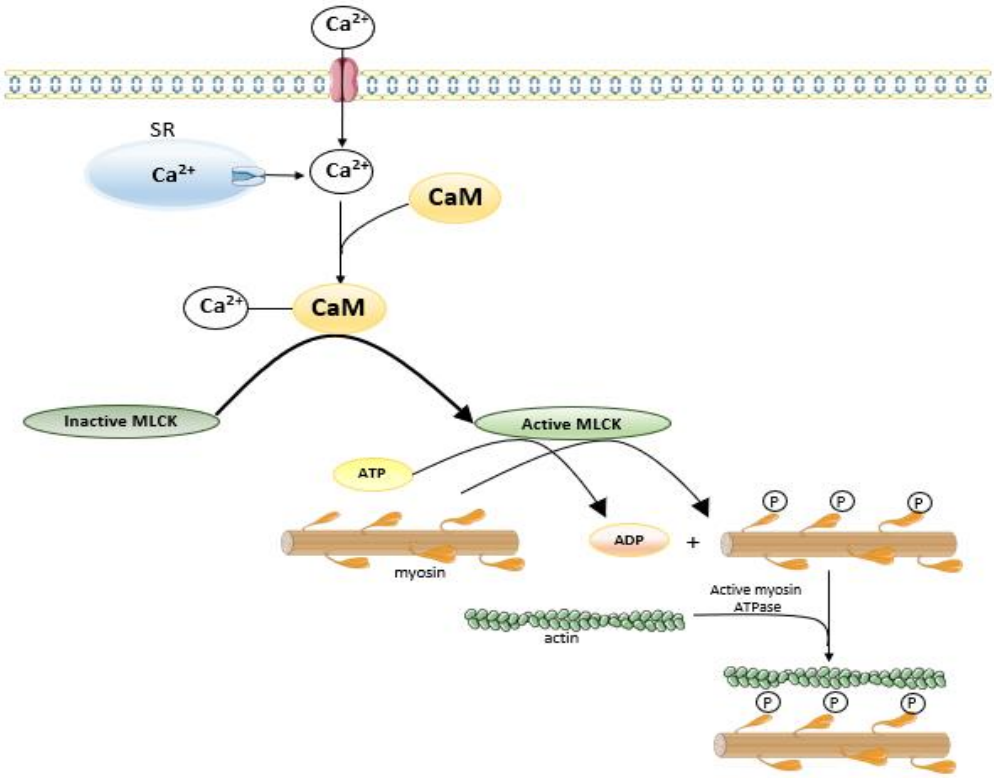

Figure 2: The mechanism of smooth muscle contraction.

Actin is a highly conserved and ubiquitous protein consisted of six different isoforms. It has been proposed that among the six isoforms of actin, four are expressed in smooth muscle. The α-smooth muscle actin (α-SMA) is the most abundant isoform in SMCs and it is responsible for the smooth muscle contraction. Actin is localized in microfilaments bundles and in association with myosin form the contractile filaments [16], [17]. The smooth muscle myosin belongs to the myosin II family and it is an essential component for the smooth muscle contraction. Smooth muscle myosin molecules are hexamers composed of two myosin heavy chains (MHCs) and four myosin light chains (MLCs). The MHCs have two distinct regions, a globular head and a helical tail. The four MLCs form two pairs consisted of namely, one essential light chain and one regulatory light chain. Each of the pair is associated with the globular heads of the MHCs. For the contraction of SMCs, it is required the phosphorylation of the regulatory light chain. Immediately after phosphorylation, cross-bridge cycling occurs, as the head region of the MHCs binds to the actin [18], [19].

Other SMC markers that are associated with the contractile function are caldesmon (CaD), calponin and smoothelin. CaD is an actin- and myosin binding protein that can be found in two isoforms, the heavy isoform (h-CaD) and the light isoform (l-CaD). The h-CaD is present in smooth muscle cells and it is considered a reliable marker for the smooth muscle differentiation whereas the second isoform, l-CaD is present in the non-muscle cells. The h-caldesmon isoform is involved in the organization and stabilization of actin filaments and regulates the interaction between actin and myosin in an inhibitory manner. This inhibitory effect is reversible after phosphorylation of the h-CaD by several kinases such as the calcium/calmodulin-dependent protein kinase II [16], [20]. Differentiated SMCs can be also identified by the expression of calponin. It is known that calponin interacts with actin and it regulates the actin-myosin interactions, but its actual functional role is a matter of controversy. Calponin exists in three isoforms: h1 (smooth muscle-specific basic), h2 (neutral) and h3 (acidic). The h1 isoform is the major isoform expressed in SMCs [16]. Finally, smoothelin is a cytoskeletal protein found exclusively in the differentiated contractile SMCs and it is characterized by its affinity to actin filaments [21].

1.2 Male urethral strictures and their management

Male urethral strictures are abnormalities which refer to a scarring process that results to the narrowing of urethra. All strictures occur after an injury at urethra and the pathogenesis of them involves the epithelium and the corpus spongiosum. The hallmark of this condition is the fibrosis within the corpus spongiosum which in the beginning can be asymptomatic; however, during the healing, this fibrosis can lead to a gradual decrease of the urethral lumen and a poorly elastic tissue. One consequential change of the urethral stricture is the reduction in the amount of collagen I followed by an increase in the amount of collagen III. This change is subsequently associated with a decrease in the population of SMCs which reside within the muscular layer of the urethra [2], [22], [23]. Furthermore, the narrowing of the urethral lumen blocks the flow of urine out of the bladder, and as a result voiding and storage symptoms, as well as urinary tract infection can arise [1], [23]. In addition, urethral strictures can lead to more serious complications such as bladder calculi, prostatitis or chronic renal failure [2]. These symptoms affect not only the health of the patients but also the quality of their life. Thus, the successful management of urethral strictures is of great importance.

Although male urethral strictures can be tackled through different invasive or surgical interventions, their effective management remains a challenge for the urologists. The gold standard for the management of urethral strictures is urethroplasty. Based on the stricture length and location, urethroplasty treatment options can vary from excision along with primary anastomosis, graft urethroplasty or the use of flaps. For short urethral strictures (<2cm), the excision of the scarred urethral part and the anastomosis of the two healthy urethral edges has shown high success rate. However, this technique comes with two limitations. First, it is only employed for bulbar strictures, and second, the erectile dysfunction of the patient is often encountered during the postoperative period. For strictures that are longer (>2cm), the augmentation urethroplasty, in which grafts or flaps are interposed, is used [2], [23]. Among the tissues that are used as grafts, oral mucosa is the most popular and versatile substitute for the treatment of urethral strictures (Figure 3). Considering the limitations of the usage of this substitute material though, such as the limited donor supply in case of long and complex urethral strictures and the donor site morbidity which is described as transient oral pain and numbness or difficulty in mouth opening later, it seems that there is a niche for synthetic repair materials [3], [9].

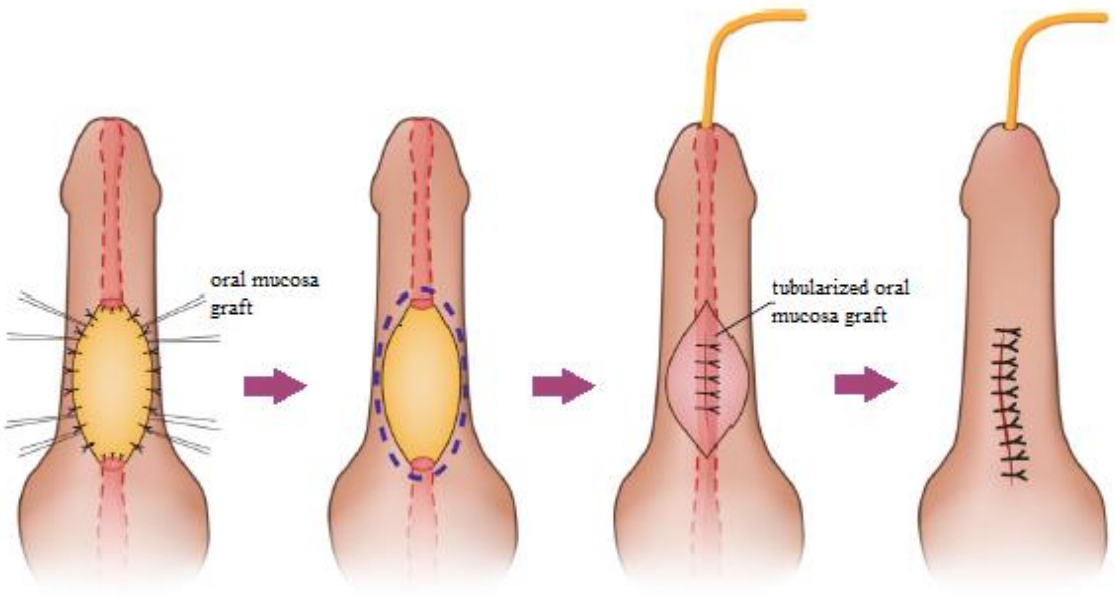

Figure 3: Example of urethroplasty for long strictures (>2cm). Modified from [24]

The use of tissue-engineered grafts as a treatment option has evoked the interest of many urologists in recent years [3]. The field of TE aims to the production of a substitute material that would be easy to handle and it would not undergo fibrosis, contraction or rejection. For this purpose, two different strategies have been employed: the first strategy involves the application of acellular scaffolds whereas the second strategy refers to the usage of cell-seeded scaffolds [4]. Scaffolds are utilized in TE to provide and support cell attachment, growth and proliferation [25]. The reconstruction of urethra with acellular scaffolds, which can be either natural or synthetic has shown a limited potential. For example, in a study with a mean follow-up of 25 months, El-Kassaby et al. used acellular bladder matrix to treat urethral strictures. In this study, the success rate was good only in patients who had a healthy urethral wound bed (8 of 9) as the success rate for patients with an unhealthy urethral wound bed was low (2 of 6) [26]. In a different study, reported by Palminteri and his colleagues, in which small intestinal submucosa was used as an acellular scaffold, the outcome was partially successful. More specifically, in patients with a stricture length less than 4cm, the successful rate was 86% whereas in patients with stricture length more than 4cm, the success rate was 0% [27].

On the other hand, cell-seeded scaffolds have shown more promising results. Raya-Rivera et al. reported a successful construction and implantation of tissue-engineered urethras in five pediatric patients after using a polyglycolic acid tubularised scaffold seeded with bladder SMCs and urothelial cells. In this study, no itra- or post-operative complications were mentioned [28]. Notwithstanding this hopeful outcome, there is a critical determinant which should be taken into consideration to conclude upon the overall efficacy of this result in the treatment of male urethral strictures. During puberty, the urethra continues to grow and double in size. As this study was conducted in pediatric patients, a further investigation for the optimal tissue-engineered scaffold synthesis and length to promote neourethral tissue regeneration is considered essential [10].

From the above data, it seems that the most optimized TE approach is the cell-seeded scaffold comparing with the acellular scaffolds. However, there are still limitations in this approach such as the difficulty of homogeneous seeding of cells onto scaffolds that should be overcome. Additionally, the controlled porosity and permeability of a scaffold, as well as a desired

distribution of multiple types of cells in the scaffold are challenges that are often met. A new technology that potentially can circumvent these problems is the 3D bioprinting [29].

1.3 3D bioprinting technology in TE

The 3D bioprinting is a pioneering technology which has gained interest as a fabrication tool for TE approaches. In this process, the deposition of biomaterials along with living cells is feasible, and through a controlled layer-by-layer manner the construction of a 3D structure, that resembles the native tissue, is achievable. Due to this accuracy, there is the possibility to use personalized data from patients and design constructs similar to patients' native tissues and organs. The 3D bioprinting process principally can be divided into three distinct steps: the pre-processing, the processing and the post-processing step. First, in pre-processing step, the digital model for the desired structure that the bioprinter will later create is chosen. The second step, which is called processing, involves the mixture of the living cells with the biomaterials called bioinks and their precise layer-by-layer deposition. Finally, the post-processing is an essential step in which the printed structures undergo maturation in order to become more stable and suitable for further *in vivo* use. The key component for the tissue maturation is a bioreactor [29], [30].

To date, three different 3D bioprinting technologies have been developed and utilized in TE field. The first attempt for tissue biofabrication employed the inkjet bioprinting technology. This technology is based on the droplet formation containing cells and the desired biomaterials. Inkjet bioprinters such as thermal or piezoelectric enable the ejection of droplets and their precise positioning onto a substrate. The second technology, which is termed extrusion, is the most common bioprinting method. Instead of droplets, bioprinters extrude continuous filaments through a nozzle, in a pneumatic or mechanical manner. The advantage of the extrusion method is that biomaterials of varying viscosity and cells in higher cell densities can be exploited compared to the inkjet method. The last and the least common technology is the laser bioprinting. This technique is a nozzle-free process in which laser pulses stimulate a "ribbon" consisting of an energy absorbing layer and a layer that comprises cells and/or biomaterials (Figure 4). This stimulation creates a high-pressure bubble which finally propels a droplet from the biological material onto a substrate [31].

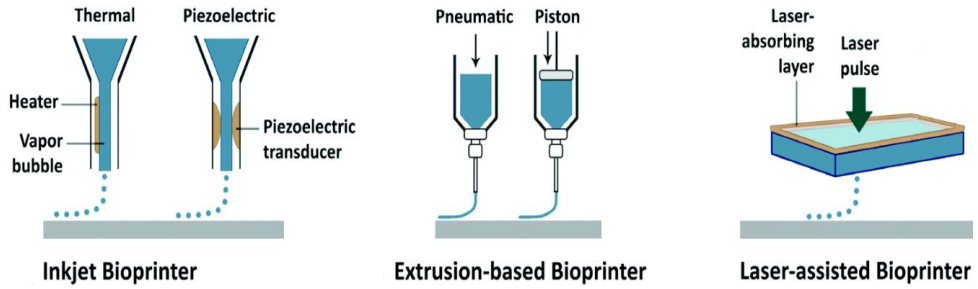

Figure 4: The three 3D bioprinting technologies. Modified from [32]

1.3.1 Biomaterials for 3D bioprinting and TE

One of the most important parameters in 3D bioprinting is the appropriate selection of a suitable biomaterial that can be used as a bioink for the printing of the desired tissue construct. A suitable biomaterial is characterized by high biocompatibility for supporting the cell adhesion,

proliferation and viability, highly mechanical stability and suitable viscosity. Materials currently used as bioinks can be obtained from either synthetic or natural resources. The advantage of synthetic biomaterials such as polyethylene glycol is that can be tailored as necessary. However, synthetic biomaterials lack specific molecular elements resulting in poor cell interactions and limited reproduction of the natural bioactive ECM environment. In contrast, bioinks based on natural resources such as alginate, collagen, gelatin and multiple others overcome these limitations [31]. For example, collagen, a main component of ECM, is present in tissues such as skin, bladder or urethra [4]. Collagen-based bioinks are of great interest as they increase the mechanical properties of 3D bioprinted constructs and support cell growth in cell-laden structures [33]. Due to its biocompatibility and the small differences in its composition among species, collagen has been extensively used as a bioink material for TE purposes [34]. A hydrolysis product of collagen, gelatin, has also gained a lot of interest in 3D bioprinting. Although at body temperature its thermal stability is poor, its ability to form hydrogels, which can be easily modified with methacrylate groups resulting in gelatin methacryloyl (GelMA), is an appealing characteristic for TE approaches. GelMa is a biomaterial with higher mechanical stability than gelatin that can also provide a propitious environment for cell growth [31]. Finally, among the natural biomaterials, alginate is a polysaccharide which can be found in brown algae. Alginate has been widely used for the 3D bioprinting of hollow and tubular constructs, as well as, has been employed for the creation of 3D neural tissue structures despite its bioinert nature. Due to its ability to entrap water and other molecules that diffuse into it, alginate is an attractive candidate as a bioink in 3D bioprinting [31], [35].

1.3.2 3D bioprinting for urethra reconstruction

To date, 3D bioprinting technology has already been utilized and showed promise within the urology field. For instance, accurate 3D printed models of patient's kidneys, delineating renal malignancies, have improved not only the patients' understanding regarding their renal pathology but also the anatomical knowledge of the clinicians [36]. Thus, their clinical value has been partly consolidated. However, regarding the application of 3D bioprinted constructs as a treatment in medical conditions, further research is required. In the field of urethral reconstruction, studies in 3D bioprinting of urethral constructs are still very limited. A recent study by Zhang et. al, which is considered the first to investigate the 3D bioprinting technique for the urethral reconstruction, demonstrated the feasibility of a 3D biomimetic urethra similar to a native rabbit urethra. In this study, bladder urothelial cells and SMCs isolated from rabbit bladder were loaded to a homogenous hydrogel composed of fibrinogen, gelatin and hyaluronic acid. Utilizing the 3D bioprinting technology, the cell-laden hydrogel was deposited on a poly (ε-caprolactone) (PCL)/ Poly (lactide-co-caprolactone) (PLCL) scaffold. Both cells types maintained their viability and proliferation capacity providing positive evidence that 3D bioprinting technology can be used in the field of urethra reconstruction [3].

This study provides strong foundation for further research in 3D bioprinting for urethral reconstruction. However, given that the goal of TE is to develop biological substitutes which can recapitulate the unique features and functions of tissues and organs, it would be of interest to investigate also the ability of SMCs to contract within a 3D bioprinted urethral construct. In this study, this critical aspect was not investigated. Moreover, although the results obtained from rabbit cells were promising, it would be optimal to examine the performance of primary human cells within 3D bioprinting technology for tissue-engineered urethral reconstruction. Primary cells taken from human tissues have more representative morphological and physical

characteristics, as well as biochemical properties than animal cells [37]. Therefore, the use of human cells obtained, for example, from a human bladder could be a better option for the creation of an urethral construct. Finally, as the scaffold approach for the biofabrication of artificial organs still faces limitations such as irritation, infection and reduced biocompatibility, a scaffold-free approach based on natural biomaterials could be another critical aspect of investigation [10].

2. Aim and Objectives of the study

Male urethral stricture resulting after urethral injury is a prevalent condition among men population which has substantial ramifications in their quality of life. In case of long urethral strictures (>2cm), current treatments such as surgery and replacement of urethral tissue face the limitation of graft failure, as well as, the shortage of donor supply. The 3D bioprinting technique and its capacity for biofabrication of tissue constructs may hold promise for functional biofabricated urethral constructs which can overcome these limitations. When bioprinting, the choice of the cell type and the selection of a suitable bioink are of great importance for a successful printing result.

Similarly to urethra, bladder is comprised of SMCs which have the physical ability to contract and relax. Therefore, the use of bladder SMCs as a cell source is an appealing and viable solution for the reconstruction of urethra. However, under culture conditions, SMCs lose their contractility introducing a new challenge within the field of urethral reconstruction. Attempts to restore SMCs functionality include chemical stimulation through soluble factors, mechanical stimulation and appropriate cell culture environment such as ideal coating reagents or 3D culture systems.

The aim of this project is to investigate the ability of SMCs isolated from human bladder tissue smooth muscle layer to retain their potential to contract and examine biomaterials that could be optimal for this purpose. The first objective of this study is to investigate the transition of the bladder SMCs towards a contractile phenotype via the induction of a differentiation culture medium under normal culture conditions. The second objective of this project is to assess the ability of two different bioinks, CELLINK and Lifeink® 200 to be extruded into stable 3D constructs supporting the bladder SMCs viability, proliferation and differentiation.

3. Materials and Methods

3.1 Cell Culture

Primary human urothelial smooth muscle cells (HUSMCs) were cultured in Ham's F12 Nutrient Mixture (Gibco, ThermoFisher Scientific) supplemented with 5% fetal bovine serum (FBS), 100 U/ml penicillin and 0.1 mg/ml streptomycin, 5µg/ml insulin, 0.5ng/ml epidermal growth factor (EGF) and 2ng/ml basic fibroblast growth factor (FGF-b), referred as growth medium (GM). HUSMCs were maintained in polystyrene flasks (Greiner Bio-one) and incubated in a standard, normoxic incubator at 37 °C, 20 % O_2, and 5 % CO_2. When reaching 80% confluence, cells were passaged. For the dissociation of cells TrypLE select (Gibco, ThermoFisher Scientific) was used. For the two-dimensional (2D) experiments, HUSMCs were seeded at a density of 20.000 cells/cm^2 in 24-well culture plates (Greiner Bio-one) coated with collagen I (Gibco, ThermoFisher Scientific) for 10 and 17 consecutive days. For the differentiation of HUSCMS, 24 hours after seeding, cells were switched to a medium composed of Ham's F12 Nutrient Mixture, 1% FBS, 100 U/ml penicillin and 0.1 mg/ml streptomycin, and 30µg/ml heparin, referred as differentiation medium (DM).

3.2 Real Time Reverse Transcription Polymerase Chain Reaction (RT-qPCR)

Total RNA was extracted from the HUSMCs cultured in the two different media, at day 0 (24 hours after seeding), 10, and 17 using an Aurum™ total RNA mini kit (Bio-rad) according to manufacturer's instructions. The concentration and the purity of the RNA in each sample were determined using spectrophotometry (NanoDrop; Thermo Fisher Scientific). High RNA values were normalized to the lowest amount of RNA within the samples. For the synthesis of the complementary DNA (cDNA), the iScript cDNA synthesis kit (Bio-Rad) was utilized.

The amplification reactions for each cDNA sample were performed in duplicates, in a final volume of 20µl per reaction consisted of cDNA, IQ SYBR Green Supermix (Bio-Rad) and the target-specific primer, on a CFX Connect Real-Time PCR machine (Bio-Rad). The PCR reactions were run using a 2-step PCR protocol, with initial denaturation at 95°C for 3 minutes followed by 40 cycles of denaturation at 95°C for 10 seconds and annealing/elongation at 60°C for 30 seconds (Table 1). A four-fold dilution series of a standard curve was prepared to enable calculation of the expression level of each gene. The expression levels of each gene were then normalized using the two housekeeping genes; Peptidylprolyl Isomerase A (PPIA) and Tyrosine 3-Monooxygenase/Tryptophan 5-Monooxygenase Activation Protein Zeta (YWHAZ).

Table 1: Primer sequences and annealing temperatures used in RT-qPCR.

Gene	Forward Primer Sequence	Reverse Primer Sequence	Annealing Temperature
α-SMA	5'-AGC-AGC-CCA-GCC-AAG-3'	5'-AGC-CGG-CCT-TAC-AGA-3'	60°C
MHC	5'-AAA-GCC-CTG-GAA-CTT-3'	5'-AGA-TTT-TGC-TCT-GCC-3'	60°C
Calponin	5'-CTG-GCT-GCA-GCT-TAT-3'	5'-CTG-AGA-GAG-TCG-ATC-3'	60°C
Caldesmon	5'-TCT-GAG-CCT-TCT-GGT-3'	5'-CCT-CGG-GAA-GAA-GTT-3'	60°C
Smoothelin	5'-TCT-GCC-AGA-TCT-GCT-3'	5'-GAA-AGG-AAC-CGA-CGG-3'	60°C
PPIA	5'-TCC-TGG-CAT-CTT-3'	5'-CCA-TCC-ACC-CAC-3'	60°C
YWHAZ	5'-ACT-TTT-GGT-ACA-3'	5'-CCG-CCA-GGA-CAA-3'	60°C

3.3 Immunofluorescence Staining

HUSMCs were washed twice with prewarmed phosphate buffered saline (PBS) and fixed in 4% formaldehyde for 15 minutes at 37°C. After washing with PBS twice to remove 4% formaldehyde, cells were permeabilized with 0.1% Triton X-100 for 5 minutes at room temperature and blocked with 1% bovine serum albumin in PBS for 30 minutes at room temperature. Subsequently, the primary antibodies; goat polyclonal anti-smooth muscle MHC 11 (ab53219), mouse monoclonal anti-smoothelin antibody [R4A] (ab8969) and the mouse monoclonal anti α-SMA antibody [1A4] (ab7817) were diluted 1:200. HUSMCs were incubated with the primary antibodies at 4°C overnight. The cells were then washed twice with PBS and incubated for 1 hour with the secondary antibodies at room temperature. For the fluorescence labeling of the desired combination of proteins, Alexa 488-conjugated goat anti-mouse (Invitrogen, ThermoScientific) and Alexa Fluor 555 goat anti-rabbit IgG (H+L) (Invitrogen, ThermoScientific), diluted 1:500, were used. Cell nuclei were stained with Hoechst 33342 (Sigma-Aldrich). All the images were captured and processed using a Zeiss AxioObserver.Z1 microscope.

3.4 Carbachol Contraction Assay

The contraction assay was performed to examine the contractile capacity of HUSMCs after cultured in DM for 17 days (Section 2.1). At day 17, HUSCMCs were washed with PBS and partially detached from the bottom of the wells after replacing PBS with a non-enzymatic cell dissociation buffer (Sigma-Aldrich) and incubating at 37°C for approximately 20 minutes. After that, the non-enzymatic cell dissociation buffer was removed and PBS was added to the wells for 30 minutes. To test and monitor the contractile capacity of HUSMCs, 100μM carbachol was added to each well and pictures were taken at 0, 5, 10 and 15 minutes after stimulation. HUSMCs cultured in GM for 17 days were used as a control. All the images were captured using a Zeiss AxioObserver.Z1 microscope. The surface area of the cells was measured and quantified using the FIJI open source software.

3.5 3D Bioprinting

All the procedures described below were carried out in a laminar flow hood under sterile conditions.

3.5.1 Preparation of cell-laden bioink

For the 3D bioprinting experiments, HUSMCs were expanded and detached as described in Section 3.1. After detachment, a cell suspension at a density of $1x10^6$ cells was transferred to a centrifuge tube. Upon centrifugation, the supernatant was removed, and the cell pellet was resuspended in 0.1mL of culture medium, GM. The amount of the GM added was calculated based on the 1:10 mixing with the bioink ratio in order to obtain the final concentration of $1x10^6$ cells/mL. To load and mix the desired number of HUSMCs with the bioink, 0.1 mL cell suspension was transferred first to a syringe and 0.9mL of the bioink was added to another syringe. After loading and extruding the air from the syringes, a coupler was attached to the end of the cell suspension syringe to connect the two syringes. The cell suspension and the bioink were mixed gently to enable a homogeneous cell dispersion within the mixture. After that, the cell-laden solution was loaded in a cartridge which was thereafter transferred to a printhead inside the BIO X 3D bioprinter (Cellink) chamber.

3.5.2 Bioprinting cell-laden constructs

For the printing of cell-laden constructs, two types of bioinks were utilized, CELLINK (Cellink) and Lifeink® 200 (Advanced BioMatrix). The bioprinting parameters were different for the two bioinks. The parameters for printing with CELLINK were set as follows: the temperature was set up to 22°C, the pressure was 25kPa, the printing speed was 8mm/s and the printhead type was pneumatic. Once the cell-laden constructs were bioprinted, they were immersed in calcium chloride solution to crosslink for 10 minutes. After 10 minutes, the cell-laden bioprinted constructs were washed once with GM and incubated under standard culture conditions until further use. For bioprinting with the Lifeink® 200, the temperature was ranging from 10-12°C, the pressure varied between 50-60kPa, the printing speed was 6mm/s and the printhead type was selected as temperature controlled. The Lifeink® 200 bioprinted constructs were crosslinked at 37°C for 45 minutes. After that time, GM was added to the constructs. Both CELLINK and Lifeink® 200 bioprinted constructs had a cylinder form (10x3mm) structured by a grid lattice and printed in 24-well plates. The type of the conical nozzles that were utilized for the bioprinting process was 22 gauge. Before and after each bioprinting experiment, the BIO X 3D bioprinter was sterilized via UV exposure.

3.6 Live/Dead Staining

To compare the effect of the two different bioinks on the phenotype of cells and assess the viability of cells, qualitatively, the Live/Dead staining was utilized. The cell-laden bioprinted constructs were washed with PBS and incubated in a serum-free solution, in this case Ham's F12 Nutrient Mixture, containing calcein AM (1 μM) and propidium iodide (15 μM) for 1 hour. After the incubation, the staining solution was removed, and the constructs were washed twice with the serum-free solution. Between each wash the samples were incubated for 15 minutes. To

evaluate the morphological changes and the viability of cells, all the samples were observed with a fluorescent microscope. The images were captured using a Zeiss AxioObserver.Z1 microscope.

3.7 Alamar blue (AB) assay

The cell proliferation in the 3D cultures was tested with the AB assay at three different timepoints; day 1, 3 and 5 after bioprinting. Prior to the experiment, the optimization of the incubation time was a critical step. The optimal incubation time was determined to be 1 hour (see Appendix A). The assay was carried out according to the manufacturer's protocol with modifications. The alamarBlue cell viability reagent (Invitrogen, ThermoFisher Scientific) was warmed at room temperature. At day 1, the alamarBlue reagent was added to each well containing a cell-laden construct, in an amount equal to 10% of the total volume in the well, and incubated for 1h at 37^{o}C. A volume of 100μl of each sample was collected and transferred to a 96-well microplate reader. Fluorescence was measured at the excitation and emission wavelength of 560nm and 610nm, respectively, using a multimode plate reader (EnSpire, PerkinElmer). After the fluorescence measurements, the cell-laden constructs were washed once with PBS. Fresh culture medium, GM, was then added and the samples were incubated at 37^{o}C. For day 3 and 5, the same process was followed. A well containing a construct without cells was used as a negative control. The fluorescence measurement of this well was subtracted as background. Based on the actual measured values of the fluorescent intensity, the proliferation of cells was expressed as doubling time, as previously reported [38].

3.8 Elastin staining

To investigate the cell maturation and differentiation of HUSMCs in the 3D cultures, an elastin staining was performed. Prior to the elastin staining, the fixation and cryosectioning of the cell-laden constructs were carried out. At day 0 and 10, medium from each well was removed, and constructs were washed twice with PBS. For the chemical fixation of the constructs, 4% paraformaldehyde (PFA) was utilized. After 1-hour incubation in 4% PFA, samples were washed twice with PBS and the second time they kept in PBS for 30 minutes. Upon removal of PBS, a further incubation with 30% sucrose solution, until constructs sank, was accomplished. In the final step, constructs were transferred on embedding cassettes covered with Tissue-Tek® O.C.T.™ Compound (Sakura) and submerged in liquid nitrogen. The frozen samples were then transferred and stored in -80^{o}C until cryosectioning and further use.
The elastin staining was performed according to the manufacturer's instructions (Sigma-Aldrich). Briefly, the sections on slides were washed with deionized water and placed in Working Elastin Solution for 10 minutes. After rinsing in deionized water until excess stain was removed, differentiation in Working Ferric Chloride Solution was accomplished. The Working Ferric Chloride Solution was washed away with tap water. Furthermore, to remove iodine, sections were first rinsed in 95% alcohol and subsequently in deionized water. Slides were then placed in Van Gieson Solution for 3 minutes, dehydrated through 95% alcohol and xylene and coverslipped after being mounted. All the images were captured using an Olympus inverted microscope.

3.9 Hematoxylin Staining

Frozen sections acquired from the cell-laden constructs cultured in GM, at day 0 and 10, were stained with Mayer's Hematoxylin (Sigma-Aldrich) and used as control to verify the results obtained from the elastin staining experiment. Briefly, the slides were rinsed with tap water and

stained with Mayer's Hematoxylin for 15 minutes. The sections then washed twice with tap water to remove the stain and 0,25% ammonia water added until the samples were colored blue. Finally, 0,25% ammonia water was removed after two washes with tap water and the sections were dehydrated through 95% alcohol and xylene. After dehydration, the sections were mounted and coverslipped. All the images were captured using an Olympus inverted microscope.

3.10 RT-qPCR in 3D bioprinted constructs

To further examine the effect of the 3D culture in the HUSMCs maturation and differentiation, an RT-qPCR was performed. Total RNA purification was completed at day 0 and 10 after bioprinting. The cell-laden constructs were detached from the wells using a steel spatula and transferred into microcentrifuge tubes. The constructs were then grinded while adding liquid nitrogen at the same time. For the total RNA extraction an Aurum total RNA mini kit (Bio-Rad) was used, and the protocol provided by the manufacturer for the extraction of total RNA from animal tissues was followed. The steps for the RNA purity, cDNA synthesis and the RT-qPCR were performed as described in Section 3.2.

3.11 Statistical Analysis

Statistical analysis was performed with GraphPad Prism 6 (GraphPad Software). Data obtained from the RT-qPCR assay were tested using a Dunn's multiple comparison test. For the results obtained from the carbachol assay Tukey's and Sidak's multiple comparison tests were performed. In all cases, a p-value <0.05 was considered statistically significant and is represented by asterisks. All data is presented as mean± standard deviation (SD).

4. Results

4.1 Investigation and comparison of HUSCMCs morphology cultured in two different media under 2D conditions

The effect of the DM on the HUSMCs towards a differentiated contractile phenotype was primarily evaluated by microscopic inspection. As can be seen from Figure 5, HUSMCs cultured in GM for 10 and 17 days grew to confluence whereas HUSMCs cultured in DM appeared less proliferative. Moreover, HUSMCs grew to GM exhibited a slender shape while lying parallel to each other. On the contrary, HUSMCs grew to DM acquired a more elongated and spindle-like shape, and appeared to be more separated from each other.

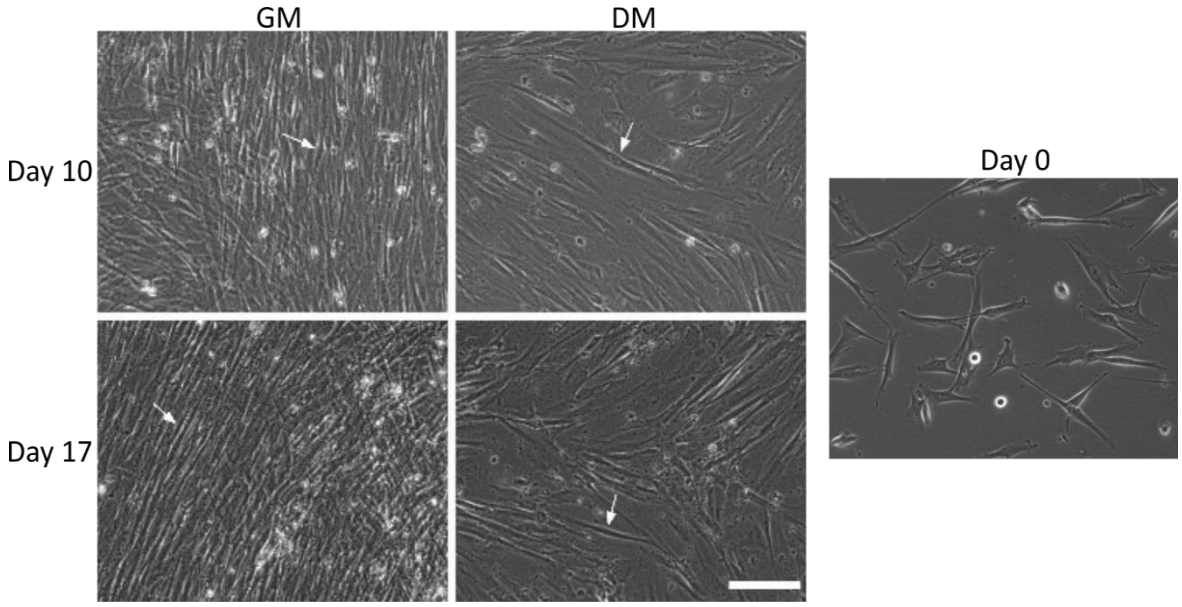

Figure 5: The effect of the different media on the HUSMCs morphology after 10 and 17 days of culture. Representative cells of each condition are shown with white arrows. Day 0 was used as baseline for a comparative cell morphology study. Scale bar: 200μm in all images.

4.2 Assessment of HUSMCs differentiation towards a contractile phenotype in 2D culture by RT-qPCR

To evaluate the effect of the DM on the induction of a contractile phenotype in HUSMCs at the transcriptional level, five contractile SMC markers (α-SMA, MHC, CaD, calponin and smoothelin) were studied. To detect changes in the expression of the genes, before and after the induction of differentiation in HUSCMCs, an RT-qPCR was conducted at different timepoints. The results are illustrated in Figure 6. The transcriptional levels of the α-SMA and calponin, in HUSMCs cultured in DM, followed an increased trend after 10 and 17 consecutive days of culture that was found to be significant compared to HUSMCs cultured in GM. When HUSMCs cultured in GM, the expression of α-SMA and calponin was increased after 10 days, though only the expression of α-SMA was found to be significantly higher. After 17 days, the expression level of both markers was decreased. As can be seen in Figure 6, the transcriptional levels of CaD followed a different pattern. HUSMCs cultured in DM, showed a significant higher expression after 17 days whereas a shortest period of culture in DM showed no significant difference. On the contrary, the expression of CaD in HUSMCs cultured in GM found to be significant higher after 10 days. In Figure 6, it can

also be seen that the smoothelin expression levels in HUSMCs cultured in DM were downregulated as wells as in HUSMCs cultured in GM for both timepoints when compared to the control. Moreover, the expression of smoothelin in HUSMCs cultured in GM for 17 days was found to be significantly decreased. The transcripts of MHC marker were not detectable and results from the RT-qPCR analysis are not shown in Figure 6.

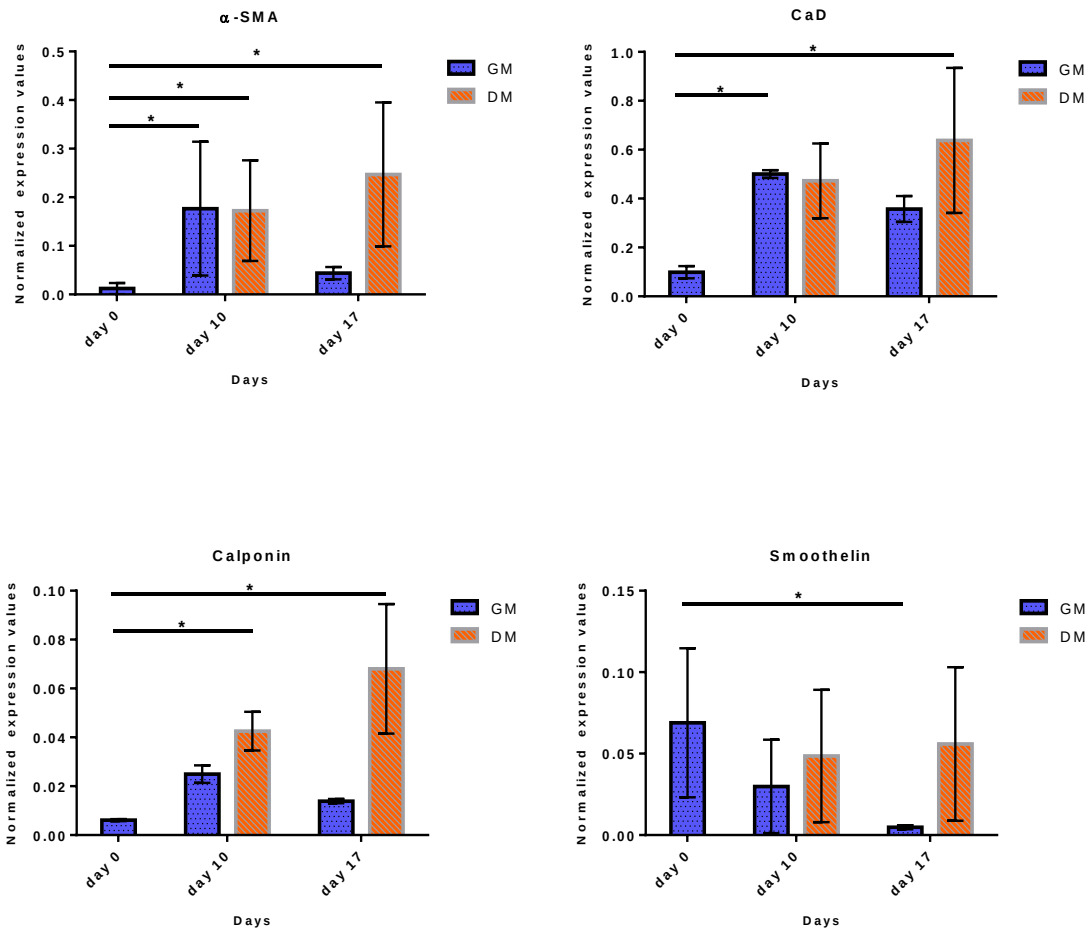

Figure 6: The effect of the GM and DM on the gene expression at transcriptional level after 10 and 17 days of culture. The results depict the normalized expression values of each investigated gene. HUSMCs cultured for 24 hours (day 0) after seeding in GM were used as control. Asterisks indicate a significant difference ($p<0.05$).

4.3 Gene expression of SMC markers at the protein level in 2D cultures

To verify the results of the RT-qPCR, immunofluorescence staining was used to assess the expression of three SMC specific contractile markers; α-SMA, MHC and smoothelin. Qualitative results after the immunofluorescence staining did not show any expression of the MHC protein after 10 and 17 days of the induction of the contractile phenotype in HUSMCs confirming the results obtained after the RT-qPCR analysis (Figure 7B, 7C). Moreover, as the RT-qPCR results showed expression of the SMC marker smoothelin at day 0, which in principle is an intermediate SMC contractile marker, staining for smoothelin was performed at this specific timepoint. However, as can be seen from the Figure 7A, smoothelin protein was not observable. On the contrary, α-SMA protein was observed in all cases (Figure 7A, 7B, 7C).

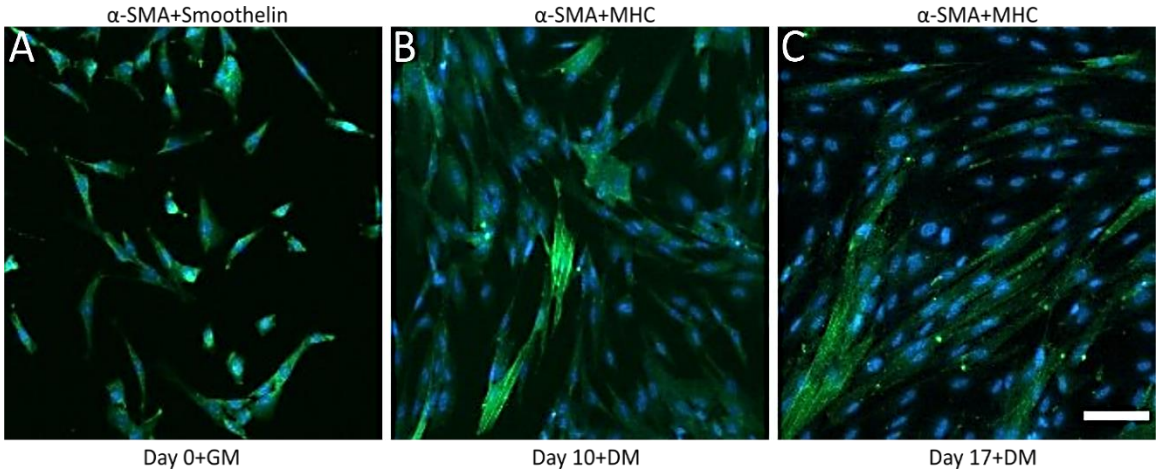

Figure 7: Immunofluorescence staining of the contractile SMC markers α-SMA (green), MHC (red), and smoothelin (red), at different timepoints. HUSMCs nuclei were stained with Hoechst 33342 (blue). Scale bar: 100μm in all images.

4.4 Assessment of contractility

To investigate the ability of HUSMCs to contract, a carbachol contraction assay was conducted. Based on the results of the RT-qPCR assay, HUSMCs cultured in DM for 17 days were chosen to be tested for their ability to contract. HUSMCs cultured in GM for 17 days were chosen as a control. Figure 8A demonstrates the effect of carbachol on HUSMCs cultured in DM for 17 days after 15 minutes of its induction and during selected timepoints. When carbachol was applied, the surface area of the cells started to decrease in length after 5, 10 and 15 minutes. However, the width of the cells was shown to be increased. After quantitative analysis of the measured cell surface area before and after stimulation with carbachol at 5, 10 and 15 minutes, the results indicated a decrease in the cell size (Figure 8B). This decrease was approximately 10% of the initial size of the cells. Tukey's multiple comparison test revealed no significant decrease in the cell surface area between the different timepoints. For HUSMCs cultured in GM for 17 days, there were also not significant differences in the cell size during the stimulation of cells with carbachol. Furthermore, when comparing HUSMCs cultured in DM with HUSMCs cultured in GM for the selected timepoints, Sidak's multiple comparison test revealed no differences in the cell sizes between the groups.

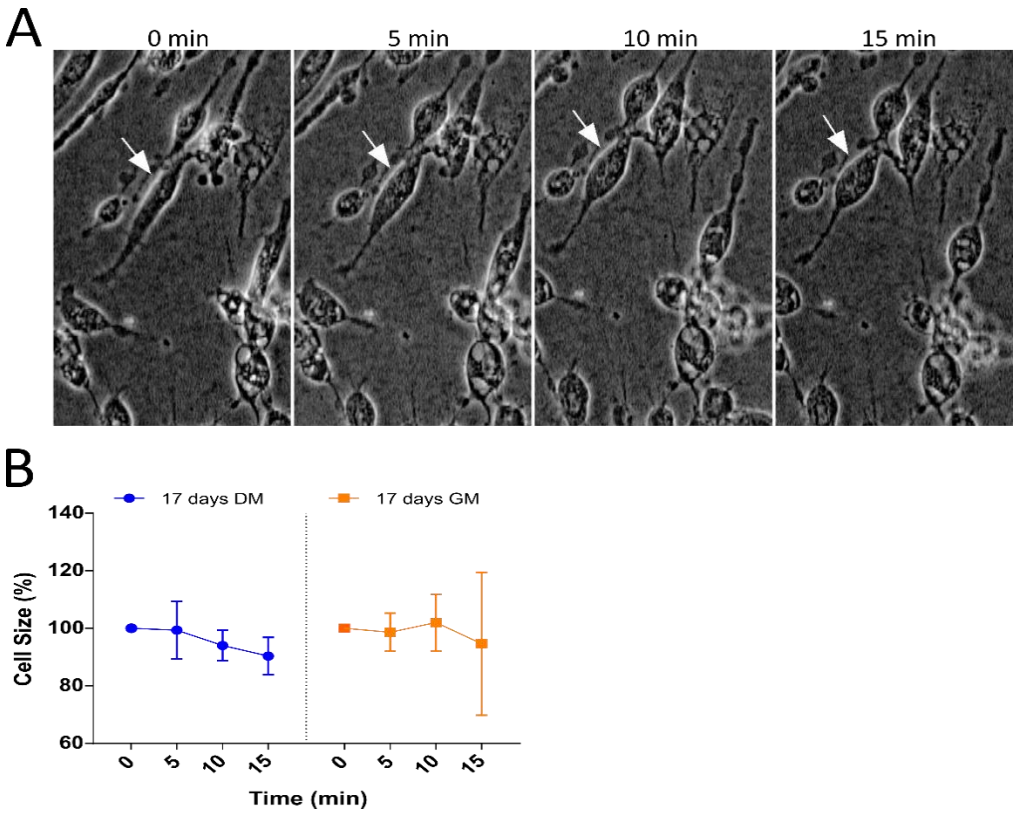

Figure 8: (A) Example of the carbachol effect on the ability of HUSMCs to contract after 17 days of culture in DM. The carbachol effect is depicted at selected timepoints. (B) Quantitative analysis of the effect of carbachol in the contraction of HUSMCs.

4.5 Assessment of 3D Bioprinting technology utilizing two different bioinks

Two different bioinks, CELLINK and Lifeink® 200, were utilized for printing cell-laden constructs, and the effect of them on the cell morphology and attachment was investigated at day 1 and 3 after bioprinting (Figure 9). At day 1, HUSMCs printed with CELLINK appeared rounded whereas the morphology of HUSMCs printed with Lifeink® 200 did not follow a uniform pattern. As can be seen from the Figure 9, most of the cells exhibited a round shape. Nonetheless, a few cells appeared more spread and elongated. At day 3, almost all cells in Lifeink® 200 obtained an elongated and spindle-like shape, while in contrast cells embedded in CELLINK maintained their rounded morphology. Based on these findings, Lifeink® 200 was deemed to facilitate better cell attachment and therefore, it was chosen for the following 3D experiments.

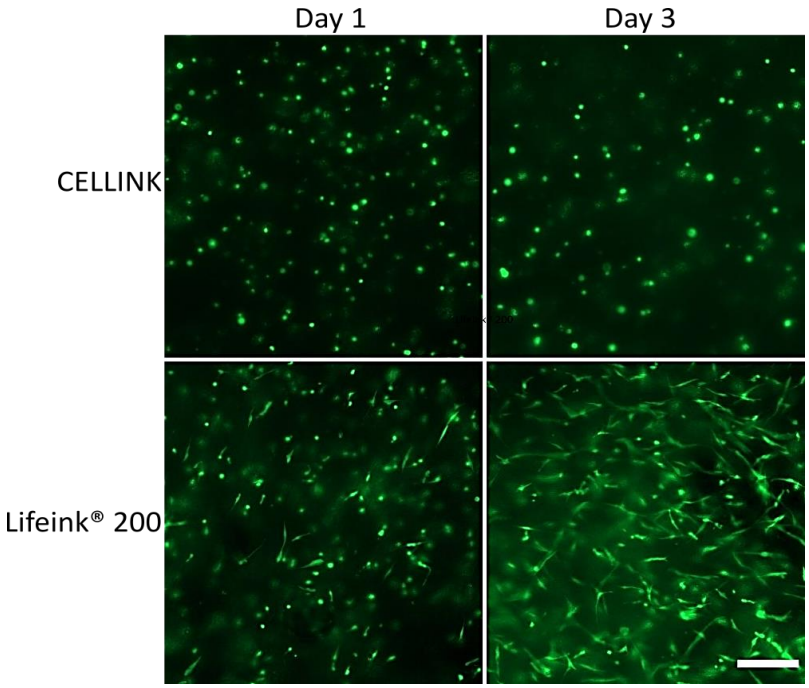

Figure 9: The effect of CELLINK and Lifeink® 200 bioinks in the morphology of HUSMCs at day 1 and 3 after bioprinting. HUSMCs were stained with calcein AM (green). Scale bar: 200μm in all images.

4.6 Evaluation of cell viability and proliferation in Lifeink® 200 bioprinted constructs

The viability of the encapsulated in Lifeink® 200 bioink HUSMCs was qualitatively assessed by the Live/Dead staining at day 1, 3 and 5 after bioprinting. As shown in Figure 10, HUSMCs retained viability over the period of 5 days. Both viable and dead cells were present in the bioprinted constructs, but live cells appeared predominant in all three different timepoints. The intense fluorescence background did not allow for an accurate and robust quantification, and thus the proliferation of HUSMCs encapsulated in the Lifeink® 200 bioprinted constructs was evaluated quantitatively by the AB assay.

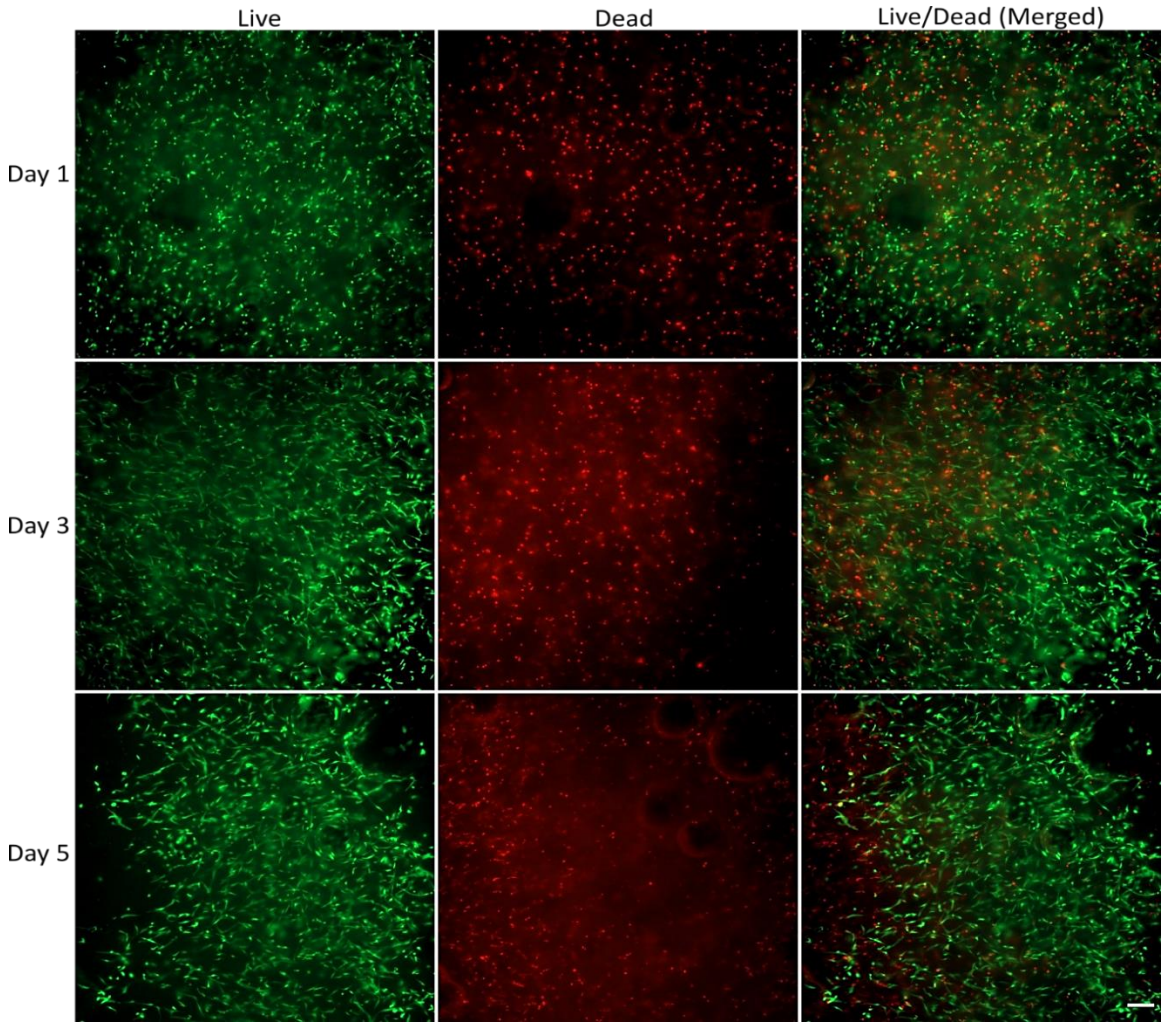

Figure 10: Live/Dead staining of encapsulated in Lifeink® 200 bioink HUSMCs at day 1, 3 and 5 after printing. Dead cells were stained red whereas live cells were stained green. Scale bar: 200μm in all images.

Figure 11 shows the averaged relative fluorescence units (RFU) that were calculated from six cell-laden bioprinted constructs. As is illustrated by Figure 11, there was an increase in the amount of RFU throughout the duration of the experiment indicating an increase in the number of live cells. To determine the rate of change in the number of live cells, the growth rate was expressed as doubling time (t_d) of the cells. The t_d was estimated to 1.55 days.

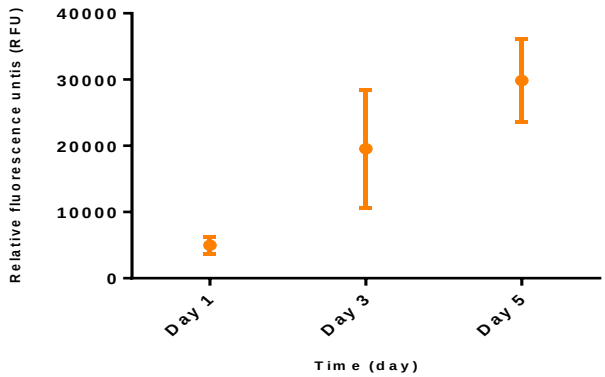

Figure 11: Averaged fluorescent intensity values and SD calculated from six Lifeink® 200 bioprinted constructs at day 1, 3 and 5 after 3D bioprinting.

4.7 Elastin deposition of HUSMCs in Lifeink® 200 bioprinted constructs

To investigate the maturation of HUSMCs in the Lifeink® 200 bioprinted constructs, sections of the structures (20μm thick) were stained for elastin at day 0 and 10, after 3D bioprinting. Results were obtained from the cell-laden bioprinted constructs cultured either in GM for 24 hours (day 0) and 10 days, respectively, or in DM for 10 days. According to manufacturer's instruction of the elastic stain kit, elastin fibers are stained black to black, nuclei are stained blue to black and collagen is demonstrated by a red color. As can be seen from the Figure 12, the visualization of collagen was highlighted by a faded red color in all cases. At day 0, in sections obtained from the Lifeink® 200 bioprinted constructs, nuclei appeared as rounded black structures that were well distributed across the constructs. Staining for elastin did not reveal any elongated structure that could be deemed to be elastin fibers. After 10 days of culture in GM, long and stretched structures were visible across the bioprinted constructs but most of them were gathered at the edge of the constructs. Based on the manufacturer's instructions and the morphology of elastin fibers, it could be hypothesized that the structures were elastin fibers. However, due to the elongated and spindle-shape morphology of HUSMCs, the black stained structures could be stained cells with a high rate of proliferation at the edge of the constructs. Comparing with HUSMCs cultured in DM for 10 days, a decreased number of nuclei were shown as black rounded structures while elastin deposition was not observed.

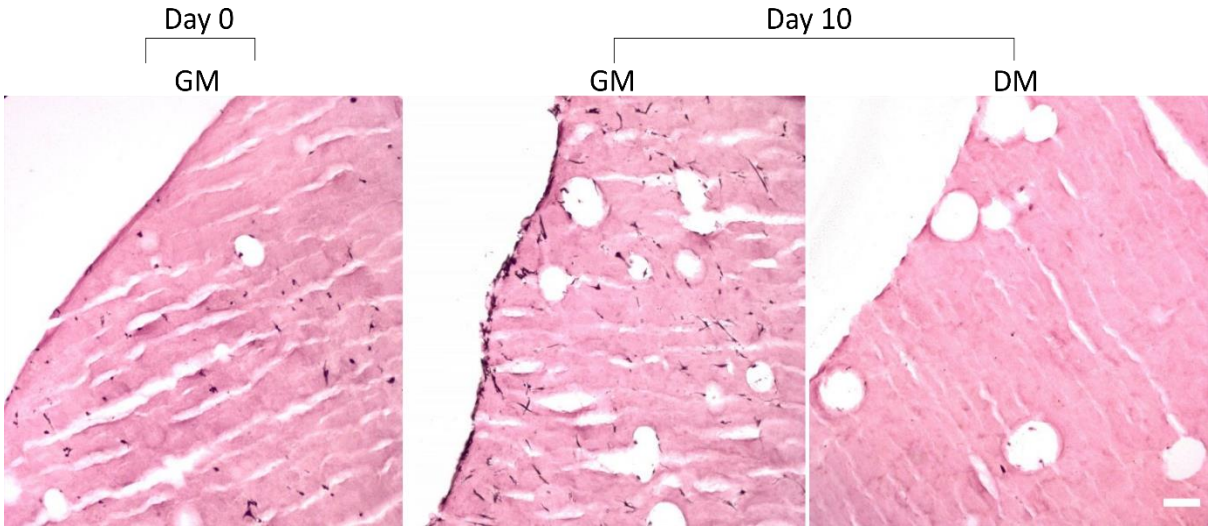

Figure 12: Sections (20μm) of the cell-laden Lifeink® 200 constructs stained for elastin. Pictures were taken after 24 hours (day 0) of HUSMCs cultured in GM, and after 10 days of HUSMCs cultured in GM and DM, respectively. The hollow structures are the result of bubble formation in the cell-laden solution. Scale bar: 200μm in all images.

4.8 Hematoxylin Staining for further evaluation of elastin deposition in the 3D bioprinted constructs

To verify, and evaluate further the results obtained from the elastin staining experiment when HUSMCs cultured in the 3D bioprinted constructs and in GM for 10 days, sections of the cell-laden constructs (20μm thick) cultured in GM were stained with hematoxylin at day 0 and 10, after bioprinting. As can be seen in Figure $13B_1$, hematoxylin, which is principally used as a stain for the nuclei of the cells, revealed dark purple structures that were distributed throughout the construct. In Figure $13B_2$, after the hematoxylin staining, dark purple elongated shapes were observed not only throughout the construct but also at the edge of it, similarly to the results

obtained after the elastin staining (Figure 13A_2). Based on the results of the hematoxylin staining, it can be concluded that after the elastin staining not elastin fibers were observed in the sections of the bioprinted constructs (Figure 13A_2).

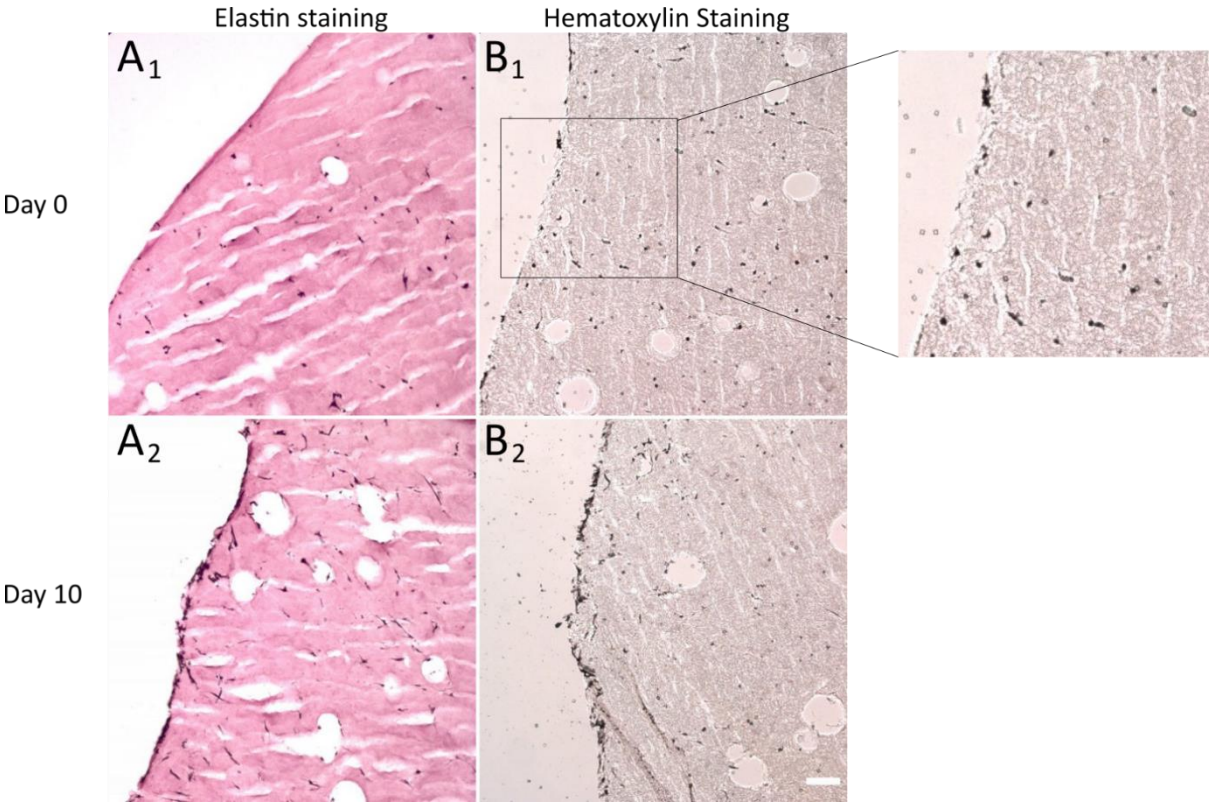

Figure 13: Sections (20μm) of the cell-laden Lifeink® 200 constructs stained with the elastic stain kit for detection of elastin deposition (A_1, A_2) and with hematoxylin for detection of nuclei (B_1, B_2). Sections were obtained from constructs where HUSMCs cultured in GM for 24 hours (day 0) and 10 days. The hollow structures are the result of bubble formation in the cell-laden solution. Scale bar: 200μm in all images.

4.9 Gene Expression of contractile SMC markers at transcriptional level under 3D culture conditions

The effect of the 3D culture in combination with different culture media, GM and DM, on HUSMCs differentiation was assessed by the expression of the five SMCs markers (α-SMA, MHC, CaD, calponin and smoothelin). Encapsulated HUSMCs cultured for 24 hours (day 0) in GM after printing were used as control. In Figure 14, preliminary results derived from an RT-qPCR can be seen. For HUSMCs cultured in the 3D cultures and in DM for 10 days, the levels expression of the genes α-SMA, CaD and calponin were significantly increased when compared to control. However, for HUSMCs cultured in 3D cultures and in GM for 10 days, although there was an increase in the expression of these three SMC markers, no significant changes were observed. Interestingly, RT-qPCR results showed an opposite effect on the expression levels of smoothelin when compared to the other genes analyzed. At 10 days after bioprinting and culturing in either GM or DM, a decrease in the levels of smoothelin expression was observed. More specifically, HUSMCs cultured in DM for 10 days found to express significantly less smoothelin when compared to control. Regarding the MHC marker, similar to the RT-qPCR analysis in 2D cultures, results from the RT-qPCR are not shown. As transcripts of the MHC marker, tested on encapsulated HUSMCs

cultured for 24 hours at GM, were not detectable, no comparison to validate the effect of the 3D culture in combination with different culture media was possible.

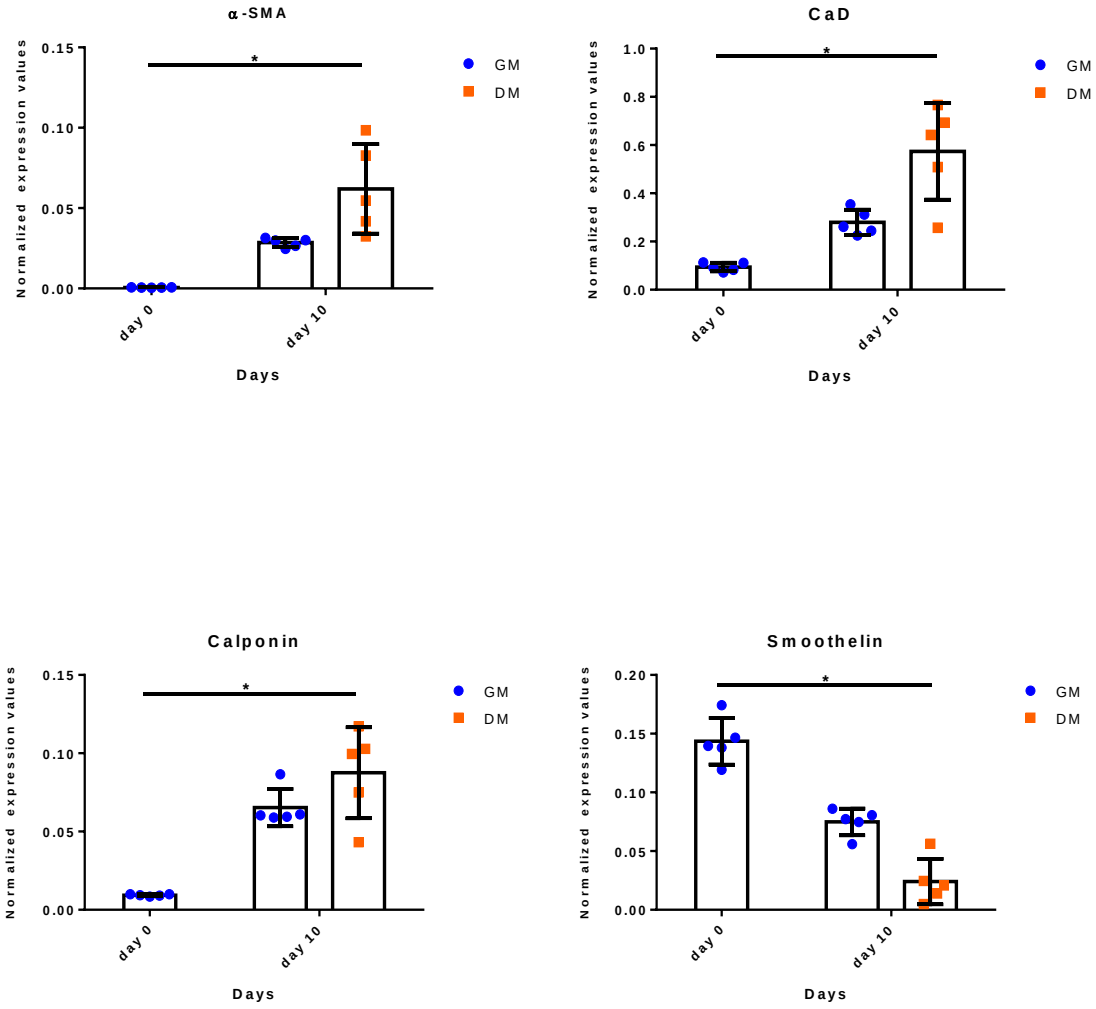

Figure 14: RT-qPCR results for the contractile SMC markers α-SMA, CaD, calponin and smoothelin. The results are the average of five replicates (constructs) of a single experiment. The expression of the genes was studied on the encapsulated HUSMCs cultured in GM and DM for 10 days. Encapsulated HUSMCs cultured for 24 hours (day 0) in GM after bioprinting were used as control. Asterisks indicate a significant difference ($p<0.05$).

5. Discussion

HUSMCs in 2D cultures

When SMCs grown in conventional 2D cell cultures, they lose their ability to contract and they shift towards a synthetic and proliferative phenotype. The ability to differentiate cultured SMCs towards a contractile phenotype remains a challenge [13]. In the present study, a medium composed of low concentration of FBS and 30μg/ml of heparin mentioned as DM was used for the induction of HUSMCs differentiation [39], [40]. It has been reported that heparin can prevent SMC proliferation [13]. Therefore, it was of interest to investigate if HUSMCs lacking the proliferative capability can exhibit a differentiated contractile phenotype. In the presence of DM, morphological changes in HUSMCs phenotype were documented when compared to HUSMCs cultured in GM. Regardless the culture time (10 days or 17 days), HUSMCs cultured in DM acquired an elongated and spindle shaped morphology, as well as they appeared less proliferative when compared to HUSMCs cultured in GM. HUSMCs grew in GM appeared slender and less elongated while they proliferated more exhibiting high cell-surface contact. While it has been reported that heparin has an anti-proliferative effect on vascular SMCs, its effect on bladder SMCs remains largely unknown [41], [42].

Given that SMC synthetic phenotype is also characterized by decreased expression of contractile SMC markers whereas the SMC contractile phenotype it can be defined by an increased expression of contractile specific SMC markers and also, their ability to contract in response to external stimuli, the second step was to study the expression of well-known SMC contractile markers [12], [13], [39]. The results for the expression of genes at a transcriptional level confirmed by an RT-qPCR. For HUSMCs cultured in either GM or DM for 10 days, the results from the RT-qPCR did not show a clear pattern. On the contrary, HUSMCs cultured in DM for 17 days had significant high levels of α-SMA, CaD and calponin expression when compared to HUSMCs cultured in GM for 17 days. These results could suggest an induction of differentiation based on DM composition and a longer culture time. However, the most intriguing findings were observed for MHC and smoothelin expression levels. The presence of both markers is the strongest evidence of a SMC contractile phenotype [43]. In the present study, the MHC gene expression results obtained from HUSCMs cultured in either GM or DM showed high quantitation cycles (Cq) irrespective of the culture duration. Moreover, at day 0, the MHC transcripts in some cases were not detectable. Due to this outcome no comparison could be made. As Cq values are inversely related to the amount of the target gene, this finding could suggest an extremely low amount of MHC transcripts in the initial sample. Another possible explanation for this finding could indicate a possible mistake in the PCR setup. Also, it should be taken into consideration that the sets of primers used in this experimental set up were predesigned and tested in human aortic SMCs. Finally, smoothelin was found to be increased after 24 hours of culture in GM while its expression followed a downward trend in all culture conditions. These results are in line with the findings of a previous study which showed that heparin detain the loss of the smoothelin in SMCs subjected to culture [44]. Additionally, they provide further support in previous results that have demonstrated that smoothelin expression is decreased throughout the culture of primary SMCs [45]. In, the present study, the expression of α-SMA, MHC and smoothelin were also verified at a translational level. As determined by the immunocytochemistry the MHC protein was absent after 17 days, but as a surprise smoothelin was also not observable at day 0.

As was mentioned above, the ability of SMCs to contract in external stimuli, such as acetylcholine, could be classified as another strong indicator for the identification of the differentiated

contractile SMC phenotype [46]. Carbachol has been shown to induce contraction to SMCs [47]. Investigating the effect of carbachol on the HUSMCs cultured in DM for 17 days at selected timepoints, no significant changes were observed. Given the absence of MHC which is the one of the two proteins that regulate the contraction in SMCs, it comes as no surprise that HUSMCs cell size were not diminished significantly.

HUSMCs in 3D cultures

A 3D cell culture can influence the cell behavior fundamentally, as it resembles an *in vivo* cell environment. Cells cultured under 3D conditions can form tissue-like constructs as they are more likely to establish cell-cell and cell-ECM interactions [48]. As 3D bioprinting technology allows for the creation of this type of culture utilizing living cells mixed with biomaterials, the second objective of this project was to assess the ability of two different bioinks, CELLINK and Lifeink® 200 to be extruded into stable 3D constructs supporting proliferation and differentiation of HUSMCs.

The choice of an ideal bioink that can support these parameters is of great importance. For the selection of the suitable bioink, the morphology of HUSMCs when bioprinted with either CELLINK or Lifeink® 200 was first taken into account. The calcein staining results revealed a potent effect of Lifeink® 200 on the morphology of HUSMCs which exhibited an elongated morphology compared to HUSMCs bioprinted with CELLINK which exhibited throughout the experiment a small, rounded shape. CELLINK is comprised of alginate and hydrated cellulose nanofibrils, whereas Lifeink® 200 is a highly concentrated collagen (35mg/ml) composed of approximately 97% collagen type I and roughly 3% collagen type III [49], [50]. Given the fact that collagen is a fibrous ECM protein which provides structural support to cells and allows for cell-surface interactions due to its surface binding constituents, it could be hypothesized that HUSMCs anchored on the edges of collagen fibers while at the same time a uniform expression of integrin molecules enabled for better adhesion [51], [52]. As urethra is a distensible structure which expands and contracts, Lifeink® 200 was chosen as the optimal bioink to continue working with for the creation of a functional urethral construct.

To investigate further the effect of Lifeink® 200 on cell behavior, the viability and proliferation of HUSMCs were assessed for up to five days after bioprinting. Both qualitative and quantitative results obtained from the Live/Dead staining and the AB assay, respectively, showed that the bioprinted Lifeink® 200 constructs support the survival and growth of HUSMCs. Considering that natural biomaterials comprised of ECM proteins are highly biocompatible, it can be reasonably assumed that this collagen-based bioink can deliver biochemical signals between cells that promote main cellular functions [53]. It has been reported that Lifeink® 200 enables cell growth and support proliferation of stem cells, as well as of the neonatal fibroblasts [54]. Moreover, Filardo et al., showed that Lifeink® 200 supported the viability of mesenchymal stem cells for up to four weeks in a study for meniscus regeneration [55]. Taken into consideration that cell viability and proliferation are key elements in TE, and an ideal cell-laden construct should promote not only the cell attachment but also the proliferation, these results indicating that the encapsulated HUSMCs can populate the bioprinted constructs suggest that Lifeink® 200 can be a promising bioink candidate for the urethral tissue regeneration [25].

The mechanical extensibility and resilience of urethra are determined by elastin [10]. Besides the well-known contractile SMC markers, proteins such as elastin is associated with the contractile phenotype of SMCs [56]. To study the effect of the 3D collagen-based environment on the differentiation of HUSMCs, the elastin deposition on the Lifeink® 200 bioprinted constructs were examined after 10 days of HUSMCs in the 3D culture. At the same time, the combined effect of DM

and the 3D culture on HUSMCs differentiation was evaluated. It has previously reported that SMCs within a collagen-matrix is more likely to exhibit a contractile phenotype [57]. However, elastin deposition from HUSMCs was not observed irrespective of the culture media. Given that elastin deposition is a barrier that TE has not circumvented yet, this finding comes as no surprise [58]. A reasonable explanation for this it could be an overexpression of GAGs from HUSMCs, that has been shown to have a potent inhibitory effect on the expression of elastin [59].

Finally, in an attempt to assess further the differentiation of HUSMCs encapsulated in the 3D bioprinted constructs, the expression of the five well-known contractile markers were confirmed by RT-qPCR. After 10 days of culture, an increase in the expression of the markers α-SMA, CaD and calponin was observed. Nevertheless, this increase was only significant for the encapsulated HUSMCs cultured in DM and not in GM. Intriguingly, the results for smoothelin showed a decrease in the smoothelin expression whereas MHC was not detectable similar to the results obtained when HUSMCs were cultured under conventional conditions. These results indicate that the combination of 3D cell culture and the DM had a positive effect on the expression of α-SMA, CaD and calponin, and possibly on HUSMCs differentiation. However, these results were limited to a transcriptional level. Reidinger and Rolle showed in their study that the expression of contractile SMC markers at a translational level occurred after 14 days when SMCs cultured in a medium for differentiation under 3D conditions [60]. Taken together these results, it can be hypothesized that although the differentiation of SMCs can be marked by the expression of specific contractile genes, the SMC functional contractility, which is defined by the contractile protein products, could occur later.

6. Study Limitations and Future Perspectives

In the present study, although heparin appeared to influence HUSMCs morphology and proliferative rate when cells cultured under 2D culture conditions, overall the ability of heparin to promote a contractile phenotype on HUSMCs was not effective. Cells did not express MHC either retain the smoothelin expression, markers which are highly definitive for contractile SMCs. Moreover, in the carbachol contraction assay, cells did not show any significant decrease in their cell size. Based on these findings, further studies should focus on the composition of a different culture medium with soluble factors that have been implicated in SMC differentiation. Moreover, the design of new primers that they meet the exact conditions and requirements of the experimental set up should have a priority.

The results obtained in the current study, regarding the assessment of the two different bioinks and their effect on HUSMCs fate, suggest that Lifeink® 200 bioink is a suitable bioink for the fabrication of the bioprinted cell-laden constructs. The Lifeink® 200 bioink had a positive effect on HUSMCs viability and proliferation although no clear effect in HUSMCs differentiation was confirmed. As elastin deposition was not observed in the cell-laden constructs after 10 days in culture and MHC was not expressed, a longer incubation time with or without an alternative differentiation culture media could be suggested. Moreover, given that male urethra is composed of three cell layers such as the inner urethral epithelium, fibroblasts and SMCs, it would be also of interest to bioprint a biological construct that consists of two or more cell types together with Lifeink® 200 bioink, and investigate the combined effect of a 3D micro-environment and co-culture in the SMC differentiation.

In conclusion, this study provides additional support in previous findings in the literature suggesting that the differentiation of SMCs cultured under conventional conditions remains a challenge. In addition, this study suggests Lifeink® 200 bioink as an optimal bioink for SMC viability and proliferation which are key elements for a tissue-engineered graft. Although the differentiation of HUSMCs encapsulated in 3D Lifeink® 200 bioprinted constructs was not confirmed in this study, there is a starting point from which further research could be undertaken for the creation of a functional biological urethral construct.

7. References

[1] A. Alwaal, S. D. Blaschko, J. W. McAninch, and B. N. Breyer, "Epidemiology of urethral strictures," *Transl. Androl. Urol.*, vol. 3, no. 2, pp. 209–213, 2014.

[2] L. A. Hampson, J. W. McAninch, and B. N. Breyer, "Male urethral strictures and their management," *Nature Reviews Urology*. 2014.

[3] K. Zhang, Q. Fu, J. Yoo, X. Chen, P. Chandra, X. Mo, L. Song, A. Atala, and W. Zhao, "3D bioprinting of urethra with PCL/PLCL blend and dual autologous cells in fibrin hydrogel: An in vitro evaluation of biomimetic mechanical property and cell growth environment," *Acta Biomater.*, vol. 50, pp. 154–164, 2017.

[4] A. Rousseau, H. Orabi, S. Chabaud, A. Morissette, S. Bouhout, and S. Bolduc, "Tissue Engineering of Urinary Bladder and Urethra: Advances from Bench to Patients," *Sci. World J.*, vol. 2013, pp. 1–13, 2013.

[5] D. R. Hickling, T.-T. Sun, and X.-R. Wu, "Anatomy and Physiology of the Urinary Tract: Relation to Host Defense and Microbial Infection," *Microbiol. Spectr.*, vol. 3, no. 4, 2015.

[6] P. Pavlica, L. Barozzi, and I. Menchi, "Imaging of male urethra," *Eur. Radiol.*, vol. 13, no. 7, pp. 1583–1596, 2003.

[7] T. L. Levin, B. Han, and B. P. Little, "Congenital anomalies of the male urethra," *Pediatric Radiology*, vol. 37, no. 9. pp. 851–862, 2007.

[8] R. T. Hoppe, T. L. Phillips, M. Roach, and Y. Yamada, "Cancer of the Male Urethra and Penis," *Leibel Phillips Textb. Radiat. Oncol.*, pp. 996–1001, Jan. 2010.

[9] J. L. H. R. Bosch, P. de Graaf, E. M. van der Linde, A. Izeta, K.-D. Sievert, P. F. W. M. Rosier, and L. M. O. de Kort, "Systematic Review to Compare Urothelium Differentiation with Urethral Epithelium Differentiation in Fetal Development, as a Basis for Tissue Engineering of the Male Urethra," *Tissue Eng. Part B Rev.*, vol. 23, no. 3, pp. 257–267, 2016.

[10] T. O. Abbas, H. C. Yalcin, and C. P. Pennisi, "From Acellular Matrices to Smart Polymers: Degradable Scaffolds that are Transforming the Shape of Urethral Tissue Engineering," *Int. J. Mol. Sci.*, vol. 20, no. 7, p. 1763, 2019.

[11] C. H. Fry, E. Meng, and J. S. Young, "The physiological function of lower urinary tract smooth muscle," *Autonomic Neuroscience: Basic and Clinical*. 2010.

[12] A. J. Halayko and J. Solway, "Invited Review: Molecular mechanisms of phenotypic plasticity in smooth muscle cells," *J. Appl. Physiol.*, vol. 90, no. 1, pp. 358–368, 2017.

[13] J. A. Beamish, P. He, K. Kottke-Marchant, and R. E. Marchant, "Molecular Regulation of Contractile Smooth Muscle Cell Phenotype: Implications for Vascular Tissue Engineering," *Tissue Eng. Part B Rev.*, vol. 16, no. 5, pp. 467–491, 2010.

[14] D. C. Hill-Eubanks, M. E. Werner, T. J. Heppner, and M. T. Nelson, "Calcium signaling in smooth muscle.," *Cold Spring Harb. Perspect. Biol.*, vol. 3, no. 9, p. a004549, Sep. 2011.

[15] D. P. Wilson, C. Sutherland, and M. P. Walsh, " Ca 2+ Activation of Smooth Muscle Contraction ," *J. Biol. Chem.*, vol. 277, no. 3, pp. 2186–2192, Jul. 2002.

[16] K. G. Morgan, S. Vetterkind, S. Appel, H. R. Kim, and S. S. Gangopadhyay, "Smooth muscle signalling pathways in health and disease," *J. Cell. Mol. Med.*, 2008.

[17] S. J. Gunst and W. Zhang, "Actin cytoskeletal dynamics in smooth muscle: a new paradigm for the regulation of smooth muscle contraction," *Am. J. Physiol. Physiol.*, 2008.

[18] T. J. Eddinger and D. P. Meer, "Myosin II isoforms in smooth muscle: heterogeneity and function," *Am. J. Physiol. Physiol.*, vol. 293, no. 2, pp. C493–C508, 2007.

[19] G. J. Babu, D. M. Warshaw, and M. Periasamy, "Smooth muscle myosin heavy chain isoforms and their role in muscle physiology," *Microsc. Res. Tech.*, vol. 50, no. 6, pp. 532–540, 2000.

[20] J. Kordowska, R. Huang, and C. L. A. Wang, "Phosphorylation of caldesmon during smooth muscle contraction and cell migration or proliferation," *J. Biomed. Sci.*, 2006.

[21] J. Krämer, C. Quensel, J. Meding, M. C. Cardoso, and H. Leonhardt, "Identification and characterization of novel smoothelin isoforms in vascular smooth muscle," *J. Vasc. Res.*, vol. 38, no. 2, pp. 120–132, 2001.

[22] A. G. Cavalcanti, S. Yucel, D. Y. Deng, J. W. McAninch, and L. S. Baskin, "The distribution of

neuronal and inducible nitric oxide synthase in urethral stricture formation," *J. Urol.*, vol. 171, no. 5, pp. 1943–1947, 2004.
[23] A. Simsek, R. Aldamanhori, C. R. Chapple, and S. MacNeil, "Overcoming scarring in the urethra: Challenges for tissue engineering," *Asian J. Urol.*, vol. 5, no. 2, pp. 69–77, 2018.
[24] A. Horiguchi, "Substitution urethroplasty using oral mucosa graft for male anterior urethral stricture disease: Current topics and reviews," *International Journal of Urology*, vol. 24, no. 7. Blackwell Publishing, pp. 493–503, 01-Jul-2017.
[25] S. Derakhshanfar, R. Mbeleck, K. Xu, X. Zhang, W. Zhong, and M. Xing, "3D bioprinting for biomedical devices and tissue engineering: A review of recent trends and advances," *Bioactive Materials*, vol. 3, no. 2. KeAi Communications Co., pp. 144–156, 01-Jun-2018.
[26] A. El Kassaby, T. AbouShwareb, and A. Atala, "Randomized Comparative Study Between Buccal Mucosal and Acellular Bladder Matrix Grafts in Complex Anterior Urethral Strictures," *J. Urol.*, vol. 179, no. 4, pp. 1432–1436, Apr. 2008.
[27] E. Palminteri, E. Berdondini, F. Fusco, C. De Nunzio, and A. Salonia, "Long-term results of small intestinal submucosa graft in bulbar urethral reconstruction," *Urology*, vol. 79, no. 3, pp. 695–701, Mar. 2012.
[28] A. Raya-Rivera, D. R. Esquiliano, J. J. Yoo, E. Lopez-Bayghen, S. Soker, and A. Atala, "Tissue-engineered autologous urethras for patients who need reconstruction: an observational study," *Lancet*, vol. 377, no. 9772, pp. 1175–1182, 2011.
[29] Y. S. Zhang, K. Yue, J. Aleman, K. M. Moghaddam, P. Assawes, S. R. Shin, M. R. Dokmeci, and R. Oklu, "3D Bioprinting for Tissue and Organ Fabrication," vol. 45, no. 1, pp. 148–163, 2018.
[30] E. S. Bishop, S. Mostafa, M. Pakvasa, H. H. Luu, M. J. Lee, J. M. Wolf, G. A. Ameer, T. C. He, and R. R. Reid, "3-D bioprinting technologies in tissue engineering and regenerative medicine: Current and future trends," *Genes and Diseases*, vol. 4, no. 4. pp. 185–195, 01-Dec-2017.
[31] Z. Xia, S. Jin, and K. Ye, "Tissue and Organ 3D Bioprinting," 2018.
[32] P. S. Gungor-Ozkerim, I. Inci, Y. S. Zhang, A. Khademhosseini, and M. R. Dokmeci, "Bioinks for 3D bioprinting: An overview," *Biomaterials Science*, vol. 6, no. 5. Royal Society of Chemistry, pp. 915–946, 01-May-2018.
[33] J. Gopinathan and I. Noh, "Recent trends in bioinks for 3D printing," pp. 1–15, 2018.
[34] S. Stratton, N. B. Shelke, K. Hoshino, S. Rudraiah, and S. G. Kumbar, "Bioactive polymeric scaffolds for tissue engineering," *Bioactive Materials*, vol. 1, no. 2. KeAi Communications Co., pp. 93–108, 01-Dec-2016.
[35] E. Axpe and M. L. Oyen, "Applications of Alginate-Based Bioinks in 3D Bioprinting," 2016.
[36] J. L. Silberstein, M. M. Maddox, P. Dorsey, A. Feibus, R. Thomas, and B. R. Lee, "Using Standard Cross-sectional Imaging and," *Urology*, vol. 84, no. 2, pp. 268–273, 2014.
[37] R. D. Combes, "The use of human cells in biomedical research and testing," in *ATLA Alternatives to Laboratory Animals*, 2004, vol. 32, no. SUPPL. 1A, pp. 43–49.
[38] C. P. Pennisi, V. Zachar, T. Fink, L. Gurevich, and P. Fojan, "Patterned polymeric surfaces to study the influence of nanotopography on the growth and differentiation of mesenchymal stem cells," *Methods Mol. Biol.*, vol. 1058, pp. 77–88, 2013.
[39] P. Chen, L. Qin, G. Li, G. Tellides, and M. Simons, "Fibroblast growth factor (FGF) signaling regulates transforming growth factor beta (TGF β) - dependent smooth muscle cell phenotype modulation," no. August, pp. 1–11, 2016.
[40] "Smooth Muscle Differentiation Supplement (SMDS) - Thermo Fisher Scientific." [Online]. Available: https://www.thermofisher.com/order/catalog/product/S0085?SID=srch-srp-S0085. [Accessed: 29-May-2019].
[41] M. Kazi, K. Lundmark, P. Religa, I. Gouda, O. Larm, A. Ray, J. Swedenborg, and U. Hedin, "Inhibition of rat smooth muscle cell adhesion and proliferation by non-anticoagulant heparins," *J. Cell. Physiol.*, vol. 193, no. 3, pp. 365–372, Dec. 2002.
[42] Y. Zhao, W. Xiao, and D. M. Templeton, "Suppression of mitogen-activated protein kinase phosphatase-1 (MKP-1) by heparin in vascular smooth muscle cells," *Biochem. Pharmacol.*, vol. 66, no. 5, pp. 769–776, Sep. 2003.
[43] S. S. M. Rensen, P. A. F. M. Doevendans, and G. J. J. M. Van Eys, "Regulation and

characteristics of vascular smooth muscle cell phenotypic diversity," vol. 15, no. 3, pp. 100–108, 2007.
[44] T. Christen, M. L. Bochaton-Piallat, P. Neuville, S. Rensen, M. Redard, G. Van Eys, and G. Gabbiani, "Cultured porcine coronary artery smooth muscle cells: A new model with advanced differentiation," *Circ. Res.*, vol. 85, no. 1, pp. 99–107, Jun. 1999.
[45] F. T. L. Van Der Loop, G. Schaart, E. D. J. Timmer, F. C. S. Ramaekers, and G. J. J. M. Van Eys, "Smoothelin, a novel cytoskeletal protein specific for smooth muscle cells," *J. Cell Biol.*, vol. 134, no. 2, pp. 401–411, Jul. 1996.
[46] K. Oishi, Y. Ogawa, S. Gamoh, and M. K. Uchida, "Contractile responses of smooth muscle cells differentiated from rat neural stem cells," *J. Physiol.*, vol. 540, no. 1, pp. 139–152, Apr. 2002.
[47] X. Su, R. Stein, M. C. Stanton, S. Zderic, and R. S. Moreland, "Effect of partial outlet obstruction on rabbit urinary bladder smooth muscle function," *Am. J. Physiol. Physiol.*, vol. 284, no. 4, pp. F644–F652, Mar. 2015.
[48] E. Knight and S. Przyborski, "Advances in 3D cell culture technologies enabling tissue-like structures to be created in vitro," *Journal of Anatomy*, vol. 227, no. 6. pp. 746–756, 2015.
[49] Cellink, "CELLINK." [Online]. Available: https://cellink.com/product/cellink-bioink/.
[50] I. Advanced BioMatrix, "Lifeink® 200." [Online]. Available: https://www.advancedbiomatrix.com/bioinks-for-3d-bioprinting/lifeink-200-concentrated-type-i-collagen-5202-1ea/.
[51] M. D. Shoulders and R. T. Raines, "Collagen Structure and Stability," *Annu. Rev. Biochem.*, vol. 78, no. 1, pp. 929–958, Apr. 2009.
[52] N. Davidenko, C. F. Schuster, D. V. Bax, R. W. Farndale, S. Hamaia, S. M. Best, and R. E. Cameron, "Evaluation of cell binding to collagen and gelatin: a study of the effect of 2D and 3D architecture and surface chemistry," *J. Mater. Sci. Mater. Med.*, vol. 27, no. 10, Oct. 2016.
[53] J. Y. Park, J. C. Choi, J. H. Shim, J. S. Lee, H. Park, S. W. Kim, J. Doh, and D. W. Cho, "A comparative study on collagen type i and hyaluronic acid dependent cell behavior for osteochondral tissue bioprinting," *Biofabrication*, vol. 6, no. 3, 2014.
[54] B. A. Bagley, "Purified Collagen Bioink for 3D Bioprinting," 2015.
[55] M. Petretta, C. Cavallo, L. Roseti, S. Durante, U. Albisinni, and B. Grigolo, "Patient-specific meniscus prototype based on 3D bioprinting of human cell-laden scaffold," vol. 8, no. 2, pp. 101–106, 2019.
[56] A. Huber and S. F. Badylak, "Phenotypic changes in cultured smooth muscle cells: Limitation or opportunity for tissue engineering of hollow organs?," *J. Tissue Eng. Regen. Med.*, vol. 6, no. 7, pp. 505–511, Jul. 2012.
[57] J. Song, B. E. Rolfe, I. P. Hayward, G. R. Campbell, and J. H. Campbell, "Effects of collagen gel configuration on behavior of vascular smooth muscle cells in vitro: Association with vascular morphogenesis," *Vitr. Cell. Dev. Biol. - Anim.*, vol. 36, no. 9, pp. 600–610, Oct. 2000.
[58] S. Hinderer, N. Shen, L. J. Ringuette, J. Hansmann, D. P. Reinhardt, S. Y. Brucker, E. C. Davis, and K. Schenke-Layland, "In vitro elastogenesis: Instructing human vascular smooth muscle cells to generate an elastic fiber-containing extracellular matrix scaffold," *Biomed. Mater.*, vol. 10, no. 3, Jun. 2015.
[59] J. Y. Hwang, P. Y. Johnson, K. R. Braun, A. Hinek, J. W. Fischer, K. D. O'Brien, B. Starcher, A. W. Clowes, M. J. Merrilees, and T. N. Wight, "Retrovirally mediated overexpression of glycosaminoglycan-deficient biglycan in arterial smooth muscle cells induces tropoelastin synthesis and elastic fiber formation in vitro and in neointimae after vascular injury," *Am. J. Pathol.*, vol. 173, no. 6, pp. 1919–1928, 2008.
[60] A. Z. Reidinger and M. W. Rolle, "Culture medium effects on vascular smooth muscle cell contractile protein expression and morphology in 2D v . 3D," pp. 8–9, 2014.

Appendix A

To test the protocol of AB assay and determine the optimal time of incubation with the alamarBlue cell viability reagent, HUSMCs response was first assessed at 2D cell cultures. HUSMCs were seeded in five different densities 25.000, 50.000, 100.000, 150.000 and 200.000 cells/well. A well containing only GM was used as negative control to subtract the background. The reading of the RFU was done in triplicates. As the correlation between the different number of cells and the RFU was linear for the 1hour-incubation, 1 hour was chosen as the optimal time for 2D cultures.

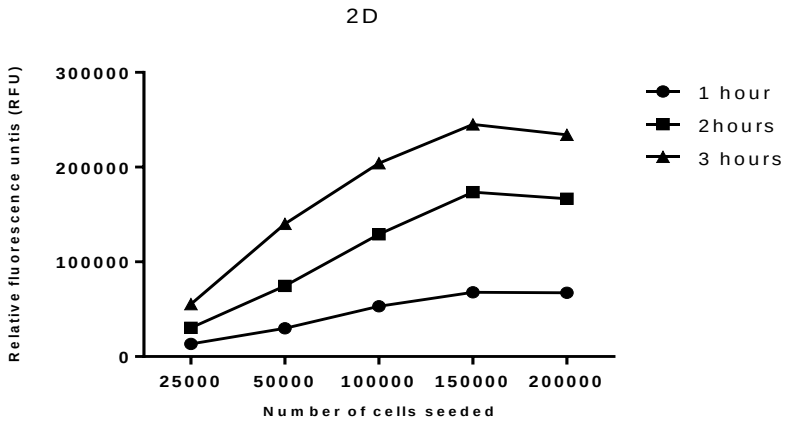

However, it was essential to optimize the incubation time within 3D cell cultures as the effect of the printing parameters on HUSMCs viability or the diffusion properties of alamarBlue cell viability reagent were not known. The AB assay was performed in triplicates for each cell number and as a negative control a well containing a construct without cells was used. To test for HUSMCs proliferation on the 3D bioprinted constructs, the 1-hour incubation was chosen as the optimal incubation time due to the approximate linear relation between the number of cells and the RFU.